Engineering xxx (xxxx) xxx

Contents lists available at ScienceDirect

Engineering

journal homepage: www.elsevier.com/locate/eng

3D Printing—Review

Process, Material, and Regulatory Considerations for 3D Printed Medical Devices and Tissue Constructs

Wei Long Ng [a,*], Jia An [b], Chee Kai Chua [b,*]

[a] Singapore Centre for 3D Printing (SC3DP), School of Mechanical and Aerospace Engineering, Nanyang Technological University, Singapore 639798, Singapore
[b] Centre for Healthcare Education, Entrepreneurship and Research @ SUTD (CHEERS), Singapore University of Technology and Design, Singapore 487372, Singapore

ARTICLE INFO

Article history:
Received 21 June 2023
Revised 18 December 2023
Accepted 16 January 2024
Available online xxxx

Keywords:
3D printing
Bioprinting
Biofabrication
Medical devices
Tissue constructs

ABSTRACT

Three-dimensional (3D) printing is a highly automated platform that facilitates material deposition in a layer-by-layer approach to fabricate pre-defined 3D complex structures on demand. It is a highly promising technique for the fabrication of personalized medical devices or even patient-specific tissue constructs. Each type of 3D printing technique has its unique advantages and limitations, and the selection of a suitable 3D printing technique is highly dependent on its intended application. In this review paper, we present and highlight some of the critical processes (printing parameters, build orientation, build location, and support structures), material (batch-to-batch consistency, recycling, protein adsorption, biocompatibility, and degradation properties), and regulatory considerations (sterility and mechanical properties) for 3D printing of personalized medical devices. The goal of this review paper is to provide the readers with a good understanding of the various key considerations (process, material, and regulatory) in 3D printing, which are critical for the fabrication of improved patient-specific 3D printed medical devices and tissue constructs.

1. Motivation

The utilization of three-dimensional (3D) printing technology for the fabrication of personalized 3D medical devices and tissue constructs represents a paradigm shift in healthcare, offering a myriad of possibilities that include replacing the once traditional one-size-fits-all approach in healthcare with a patient-centric model that is tailored to the unique physiology and requirements of each patient. The 3D printed medical devices are physical instruments or tools that can be used to diagnose, treat, or prevent medical conditions which include medical implants [1], surgical models [2], surgical instruments, and personal protective equipment [3], whereas the 3D bioprinted tissue constructs can be fabricated using patients' cells, are primarily used for repair and reconstruction of a recipient's tissue [4–8]. The 3D printing technology provides a versatile and highly automated platform for the fabrication of patient-specific 3D medical devices or tissue constructs with unprecedented precision and complexity. The key motivation behind the integration of 3D printing into the medical field includes the ability to design and fabricate bespoke 3D medical devices, implants, and prosthetics that seamlessly conform to a patient's anatomy.

The global market for 3D-printed medical devices is expected to grow from 2.7 billion USD in the year 2022 to 6.9 billion USD in the year 2028 at a compound annual growth rate of 17.1% [9]. There is a high demand for 3D-printed personalized medical devices or tissue constructs due to ①customization, ②increased complexity, and ③print-on-demand ability. Notably, the development and production of 3D-printed medical devices and tissue constructs involve complex considerations related to processes, materials, and regulatory requirements. These aspects are crucial for ensuring the safety, efficacy, and quality of the 3D printed parts and an in-depth understanding of these key considerations is vital for the development of safe, effective, and high-quality 3D medical devices and tissue constructs that meet the requirements of patients while complying with regulatory guidelines. This review article aims to highlight and discuss the various key considerations for the fabrication of 3D personalized medical devices and tissue constructs in terms of process, material, and regulatory considerations in the subsequent sections.

* Corresponding authors.
E-mail addresses: ng.wl@ntu.edu.sg (W.L. Ng), cheekai_chua@sutd.edu.sg (C.K. Chua).

https://doi.org/10.1016/j.eng.2024.01.028

Please cite this article as: W.L. Ng, J. An and C.K. Chua, Process, Material, and Regulatory Considerations for 3D Printed Medical Devices and Tissue Constructs, Engineering, https://doi.org/10.1016/j.eng.2024.01.028

2. Publication landscape on 3D printing techniques

There are 7 key 3D printing techniques based on the American Society for Testing and Materials (ASTM) standard classification (material extrusion, material jetting, powder bed fusion, vat photopolymerization, binder jetting, directed energy deposition (DED), and sheet lamination) as shown in Fig. 1(a) and there is an increasing number of publications on 3D printed medical devices and tissue constructs over the last decade according to Web of Science using the following keywords: "3D printed" + products – "medical implants", "surgical models", "surgical instruments", "personal protective equipment" or "tissue constructs" (Fig. 1(b)). Further analysis on the 3D printing techniques for fabrication of 3D printed medical devices or tissue constructs was performed on Web of Science using the following keywords: "3D printed" + 3D printing technique (① material extrusion – "extrusion," ② material jetting – "jetting," ③ powder bed fusion – "selective laser melting," "direct melt laser sintering," "selective laser sintering" and "electron beam melting," ④ vat photopolymerization – "stereolithography" and "digital light processing," ⑤ "binder jetting," ⑥. "directed energy deposition" and ⑦. "sheet

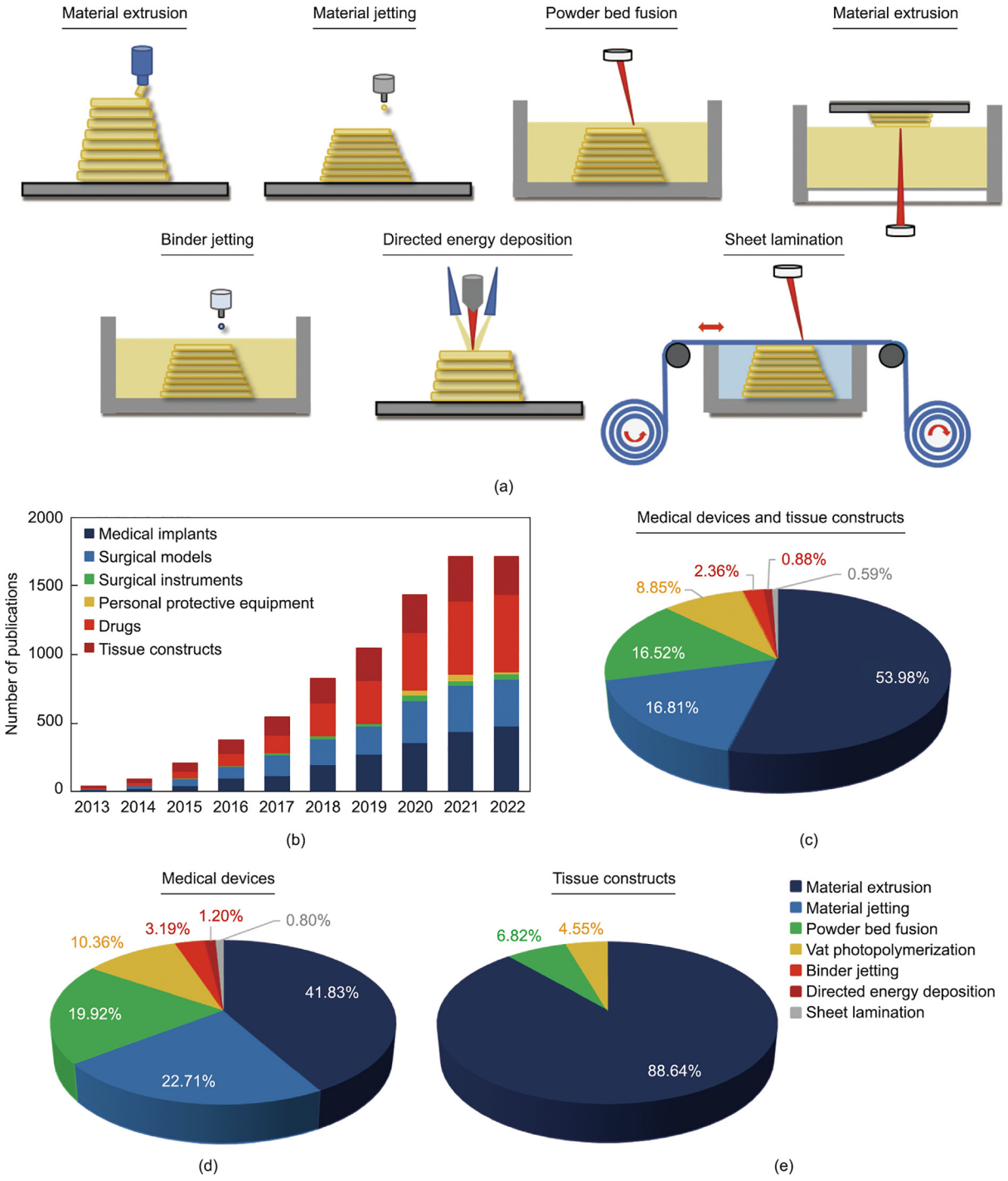

Fig. 1. (a) There are 7 different types of 3D printing techniques—material extrusion, material jetting, powder bed fusion, vat photopolymerization, binder jetting, DED, and sheet lamination. (b) Number of publications on 3D printing of medical devices and tissue constructs over the last decade. Analysis of 3D printing techniques for fabrication of (c) both medical devices and tissue constructs, (d) medical devices, and (e) tissue constructs.

lamination") + medical devices – "medical implants," "surgical models," "surgical instruments," "personal protective equipment" or "tissue constructs." Our preliminary results reflect the general publication landscape for 3D printed medical devices and tissue constructs; the most used 3D printing technique for fabrication of medical devices and tissue constructs is material extrusion (53.98%), followed by powder bed fusion (16.81%), vat photopolymerization (16.52%), material jetting (8.85%), binder jetting (2.36%), directed energy deposition (0.88%), and lastly sheet lamination (0.59%) (Fig. 1(c)). All seven types of 3D printing techniques can be used for fabrication of 3D printed medical devices—material extrusion (41.83%), powder bed fusion (22.71%), vat photopolymerization (19.92%), material jetting (10.36%), binder jetting (3.19%), directed energy deposition (1.2%) and sheet lamination (0.8%) (Fig. 1(d)), whereas only material extrusion (88.64%), vat photopolymerization (6.82%), and material jetting (4.55%) are suitable for fabrication of 3D bioprinted cell-laden tissue constructs (Fig. 1(e)). It is important to note that further scientometric analyses are required for more detailed and in-depth investigations, which have been published elsewhere [10]. In the following sections, a more comprehensive discussion of process considerations, material considerations, and regulatory considerations of various 3D printing techniques will be presented.

3. Process Considerations

3.1. Different 3D printing processes

3.1.1. Material extrusion

Material extrusion is the most used 3D printing technique, and it is commonly used for fabrication of 3D printed medical devices such as prosthetics [11–13], orthopedic implants [14–16], surgical guides [17–19], surgical models [20–22], customized personal protective equipment [23,24] and tissue-like constructs (e.g., bone [25–28], cardiac [29–32] and cartilage [33–35]). Some of the commonly used materials include polymers—hydrogels [36–40] or thermoplastics [41], metals [42,43], and even ceramics [44,45] (Table 1). In the material extrusion-based process, the material is selectively extruded through a nozzle or orifice to fabricate complex 3D printed parts in a layer-by-layer deposition approach [46]. The material extrusion-based process can be categorized into two broad groups which involve ① material melting and deposition at high temperatures—fused deposition modeling (FDM)/fused filament fabrication/screw-assisted additive manufacturing [47,48], ② pneumatic or mechanical-based material extrusion—direct ink writing, melt electrospinning writing [49–52].

The material melt extrusion-based approach is dependent on numerous processing parameters which include temperature (nozzle, print bed, and chamber), nozzle speed, and slicing thickness [53–56]. An optimal nozzle temperature (just below the material decomposition temperature) helps to enhance the weld strength of 3D printed parts; a study investigated the influence of nozzle temperature (210–250 °C) on the weld strength of acrylonitrile butadiene styrene (ABS) filament (has a range of decomposition temperatures beginning from 360–450 °C [57]) and it reported that a maximum weld strength was obtained at the highest nozzle temperature (250 °C) [58]. An optimal print bed temperature (dependent on the type of filament) facilitates improved adhesion of 1st initial printed layer and minimizes the accumulation of thermal stress within the 3D printed parts [59,60]. The optimal print bed temperature varies with the type of filament being used; a bed temperature of 115 °C was used for ABS filament [59], whereas a bed temperature close to room temperature was used for both neat polypropylene and glass-reinforced polypropylene [60]. The bed temperature is usually lower than the nozzle temperature to initiate the setting process for material solidification. Furthermore, an increase in the layer thickness can help to improve the elastic modulus [61]. The dimensional accuracy of the printed parts in a material extrusion-based process is determined by various material- and process-related parameters such as material shrinkage [62] and chamber temperature [63]. The surface finishing of the final 3D material-extrusion printed parts can be improved by optimizing the process parameters [64], the slicing strategy [65,66], the part build orientation [67,68], and chemical treatment [69,70]. The surface finish, build time, and support structure are considered guidelines for deciding an optimal part orientation; it helps to minimize or eliminate excessive supporting structures and improves the overall surface finishing [71].

Extrusion-based bioprinting is a 3D printing technology specifically designed for the fabrication of complex 3D tissue constructs using biological materials such as living cells and biomaterials. Some important process considerations during hydrogel extrusion-based bioprinting of tissue constructs include bio-ink printability [72], shear stress [73,74], and potential nozzle clogging [75]. The bio-ink printability in extrusion-based printing can be represented by the loss tangent value ($\tan\delta$)—which can be defined as the ratio of loss modulus (G'') to storage modulus (G') and printing within a suitable "printability window" is important for obtaining 3D tissue constructs with good shape fidelity. Next, the cell viability during the extrusion-based printing process is dependent on the shear stress experienced by the encapsulated cells within the extruded bio-inks, which is affected by the bio-ink viscosity, nozzle geometry, nozzle diameter, and printing pressure. There is also a potential issue of nozzle clogging when printing cell-laden bio-inks of high cell concentration using small nozzle diameter ($\sim$100 μm). The optimal viscosity of a printable bio-ink is within 10^1–10^7 mPa•s [76] and a maximum concentration of $\sim 10^7$ cells·ml^{-1} (high cell-laden bio-inks may interfere with hydrogel formation) [77,78]. The different types of cell-laden bio-inks used in extrusion-based bioprinting include alginate-based (5%–8% w/v) [79,80], gelatin-based (5%–10% w/v) [81–86], hyaluronic acid-based (1.5%–2.5% w/v) [87–90], polyethylene glycol (PEG)-based (20% w/v) [91] and Pluronic F-127 ($\geq$ 20% w/v) [92,93]. Furthermore, decellularized extracellular matrix (dECM) bio-inks derived from various tissues/organs are typically printed using extrusion-based bioprinting at 1%–4% w/v concentration [94]. The dECM bio-inks are usually printed at a low temperature of $\leq$15 °C to mitigate pre-gelation and the temperature-dependent crosslinking occurs at 37 °C.

3.1.2. Powder bed fusion

Powder bed fusion is the 2nd most used 3D printing technique (16.81%); it can be used for the fabrication of 3D printed medical devices such as orthopedic implants [95–97], dental implants [98–100] and surgical instruments [101,102] and a wide variety of powders (polymers, metals, and ceramics) can be processed [103–107] (Table 1). During the printing process, thermal energy is used to selectively fuse regions of a powder bed that are spread onto the building platform to obtain the 3D finished parts. The printing commences with orientating a pre-defined 3D computer-aided design (CAD) model within the build volume along with its supporting structures under inert conditions, scanning the scan path with a pre-defined combination of printing parameters, and lastly recoating with a fresh layer of powder particles [103]. Examples of powder bed fusion processes include: ① selective laser melting (SLM), ② direct melt laser sintering (DMLS), ③ selective laser sintering (SLS), and ④ electron beam melting (EBM) [103,104]. The key difference between SLM and DMLS is the temperature used to process the powders—the powders are fully melted at high temperatures in SLM to achieve a molten state,

Table 1
Analysis of different 3D printing techniques for fabrication of medical devices and tissue constructs.

3D printing techniques	Process	Printing parameters	Printing speed and resolution	Materials	Support structures	Applications	References
Material extrusion	Dispensing material in the form of filaments/ strands through a nozzle	Temperature, layer thickness, printing speed, material-substrate interaction	Speed: √ √ √ Resolution: Dependent on nozzle size (200–1200 μm)	Polymers (ABS, ASA, Nylon 12, PC, PEI/ULTEM, PLA, TPU, PEEK, and hydrogels) Metals (a mixture of metal powder with PLA/ABS, metallic glasses) Ceramics (Zirconia/methylcellulose paste, calcium silicate/strontium phosphate/polyvinyl alcohol slurry)	Yes	Medical devices Tissue constructs (40%–80% cell viability [261])	[42–45,53–56]
Powder bed fusion	Fusing material using thermal energy from the laser source	Laser power, powder recoating, coalescence and cooling, laser-powder interaction	Speed: √ √ Resolution: Dependent on beam spot size, powder size, scanning speed (50–100 μm)	Polymers (Polyamides – PA 11 and PA12, polystyrene, PCL, PLA, PLLA, and PEEK) Metals (Several types of steels, titanium and its alloys, nickel-based alloys, cobalt–chrome, silver, and gold) Ceramics (Aluminum oxide, titanium oxide, and calcium hydroxyapatite)	Yes (Metals and ceramics) No (Polymers)	Medical devices	[103–108]
Vat photopolymerization	Crosslinking of liquid photopolymer resin using light source	Laser power, irradiation time, resin viscosity, PIs, reducing photo-absorbers, laser-resin interaction	Speed: √ √ Resolution: Dependent on laser spot size, irradiation time (20–50 μm)	Polymers (acrylic/epoxy-based resins, hydrogels) Metals (Tungsten carbide/cobalt-based, silver acrylate/methacrylate-based, and copper-based resin) Ceramics (Alumina-based, silica-based, and zirconium silicate-based resin)	Yes	Medical devices Tissue constructs (~80% cell viability [261])	[136–142]
Material jetting	Contactless dispensing of materials in the form of droplets (pL or nL)	Ink viscosity, surface tension, density, nozzle diameter, particle size, droplet-substrate interaction	Speed: √ √ Resolution: Dependent on nozzle size, droplet-substrate interaction (15–30 μm)	Polymers (Thermoplastics—mixtures of wax and polymer, hydrogels) Metals (Copper, aluminum, tin, and alloys) Ceramics (Zirconia, alumina)	Yes	Medical devices Tissue constructs (> 85% cell viability [261])	[172–180]
Binder jetting	Dispensing binder to fuse the adjacent powder particles	Powder flowability, binder printability, binder-powder interaction	Speed: √ √ Resolution: Dependent on nozzle size, powder size, droplet-powder interaction (30–60 μm)	Polymers (Starch/plaster-based, poly-methyl methacrylate) Metals (Steel-, nickel-, cobalt-, titanium-, aluminum-, copper-based alloys) Ceramics (Silicon carbide, boron carbide, alumina, and zirconia)	No	Medical devices	[221–227]

Table 1 (*continued*)

3D printing techniques	Process	Printing parameters	Printing speed and resolution	Materials	Support structures	Applications	References
DED	Simultaneous melting of deposited material using focused thermal energy	Laser attenuation, powder size, and geometry, laser-powder interaction	Speed: √ √ √ √ Dependent on laser spot size, powder size, scanning speed (100–500 μm)	Metals (Most metals are quite straightforward to process, except certain metals like gold, alloys of aluminum, and copper with high reflectivity and thermal conductivity) Ceramics (Difficult to process as few can be heated to form a molten pool)	No	Medical devices	[253–257]
Sheet lamination	Bonding multiple material sheets of pre-defined shape/geometry	Laser power, scanning speed, bonding mechanism	Speed: √ √ √ √ √ Dependent on layer thickness, the bonding method	Polymers (Polyvinyl chloride (PVC) sheets) Metals (Aluminum and low-carbon steel materials are commonly used) Ceramics (Silicon carbide, titanium carbide-nickel, composite, and aluminum oxide)	No	Medical devices	[259,260]

ASA: acrylonitrile styrene acrylate; PC: polycarbonate; PEI/ULTEM: polyetherimide; PLA: polylactic acid; TPU: thermoplastic polyurethane; PEEK: polyether ether ketone; PA: polyamide; PCL: polycaprolactone; PLA: polylactic acid; PLLA: poly(L-lactic acid).

whereas the powder surfaces weld together during DMLS at a lower temperature [105]. The laser-based powder bed fusion processes are usually performed in an inert environment, whereas the electron-based powder bed fusion process is performed within a vacuum chamber [103]. Furthermore, each layer of powders in the EBM process is lightly sintered to minimize the build-up of electrostatic charges and repulsion of powder particles before subsequent scanning over the same toolpath to fuse the sintered powders. The excessive powders are removed via vacuum and further post-processing methods such as coating, sintering, or infiltration are performed.

Some critical process/material parameters for the powder bed fusion printing approach include energy input, powder recoating, coalescence, and cooling [108]. The advantages of the powder bed fusion printing approach include the fabrication of complex structures with good surface finishing without the need for supporting structures (especially for polymer), whereas the limitations include low fabrication speed due to slow powder recoating speed and laser scanning speed. Some recent strategies to achieve 3D printed parts with improved density and surface finishing at a higher throughput rate involved mitigating the build-up of thermal stress and eliminating crack initiation and propagation via a re-melting approach [109–111] and implementation of multi-laser scanning to improve the fabrication speed [112–114].

3.1.3. Vat photopolymerization

Vat photopolymerization is the 3rd most used 3D printing technique (16.52%); it can be used for fabrication of 3D printed medical devices such as orthodontic devices [115–117], hearing aids [118] and surgical guides [119–121], and tissue constructs (e.g., bone [122–125], cartilage [126–128], liver [129–131], and neural tissues [132–135]). The different materials used in vat photopolymerization include polymer resins [136,137], metallic- [138–140], and even ceramic- [140–142] containing suspensions (Table 1). The photo-curable resin is selectively crosslinked when a light source is projected onto the surface to initiate the free-radical photopolymerization process to obtain the completed 3D parts [136]. The vat photopolymerization process can be classified into 2 main groups: stereolithography (SLA) and digital light processing (DLP) and it can be further categorized based on the position of the light source – bottom-up or top-down. The light source is positioned below the bottom of the vat through a window to crosslink the resin in the bottom-up SLA printing process, whereas the light source is positioned directly above the vat and building platform to crosslink the resin in the top-down SLA printing process. A digital micromirror device (DMD) is commonly used in the DLP process to facilitate rapid crosslinking of a single resin layer as compared to a single beam spot in SLA, which resulted in significantly faster fabrication speed for DLP [143]. Notably, an optimal irradiation duration ensures sufficient macromer conversion to achieve strong interface bonding at the layer interface while minimizing over-exposure to prevent undesirable partial polymerization of surrounding resin. A recent study has demonstrated that the optimal UV exposure time for the fabrication of polydimethylsiloxane (PMDS) structures with a high aspect ratio was 2.5 s for each printed layer [144]. A resin with a high molar extinction coefficient (ε) would facilitate crosslinking of a smaller voxel volume and mitigate over-curing. The light penetration depth can be increased by decreasing the photo-initiator (PI) concentration or reducing dyes/photo-absorbers. The addition of a non-reactive dye component or photo-absorber within the resin improves the printing resolution as it competes with the PI in light absorption. Some key considerations for the vat photopolymerization process include the laser source, printing parameters, vat design, resin viscosity, laser-resin interaction, and formulation of photo-curable resins (biocom-

patibility, solvent used, and the formation of free-radical by-products) [136].

Unlike other bioprinting techniques (extrusion-based and jetting-based bioprinting) that deposit living cells via a nozzle, vat photopolymerization-based bioprinting uses biocompatible liquid bio-resins for the fabrication of intricate 3D cell-laden tissue constructs at high cellular density [145]. Some important process considerations during vat photopolymerization-based printing of tissue constructs include the use of suitable laser wavelength [146,147] and biocompatible PI [148]. It has been reported that shorter wavelength is more detrimental to the living cells as the higher amount of energy leads to increased DNA cellular damage. Furthermore, an ideal PI should be highly hydrophilic (the presence of more hydrophilic groups decreases the cellular uptake of PIs and reduces the cytotoxicity effect on living cells) [149,150] and crosslink at long wavelengths (formation of UV-initiated free radicals at short wavelengths has the most detrimental effect on the cell viability) [148]. Significant progress has been made in the vat photopolymerization-based bioprinting technique and it is particularly valuable for the fabrication of complex 3D tissue constructs with high-resolution structures at high cell density. The different types of bio-inks used in vat photopolymerization-based bioprinting include alginate-based (5%–8% w/v), gelatin-based (2.5%–15% w/v) [151–153], and PEG-based (10% w/v) [154].

3.1.4. Material jetting

Material jetting is the 4th most used 3D printing technique (8.85%), and it can be used for the fabrication of 3D printed medical devices such as orthodontics devices [155–157], anatomical models [158–160], and tissue constructs (e.g., alveolar lung [161–164], retina [165–168], and skin [169–172]) (Table 1). Different types of printable materials using the material jetting-based systems include polymers [172–174], metallic- [175–177], and even ceramic- [178–180] containing suspensions. In the material jetting-based process, discrete droplets are selectively deposited onto an underlying substrate surface to fabricate the 3D-printed part. There are different variants of material jetting-based systems which include inkjet-based (continuous or drop-on-demand (DOD)) [181] and electrohydrodynamic jetting [182]. During the printing process, the printhead moves horizontally to deposit the functional ink droplets (typically in the picolitre – pL or nanolitre – nL range). The applied pressure pulse from the actuator overcomes the surface tension of the ink to eject discrete ink droplets from the nozzle orifice. The deposited droplets on the substrate surface would coalesce and crosslink to form the desired shape in that layer, droplets for the subsequent layer are then deposited onto the preceding layer to eventually obtain the 3D finished parts.

The printability is influenced by the physical properties of ink (viscosity, surface tension, and density) and nozzle radius and it can be represented by the inverse of Ohnesorge number (Oh)—Z value (defined as the ratio between the Reynolds number and square root of the Weber number) can be used to represent the ink printability in the material jetting-based process [183]. The nozzle size has a significant influence on the printing resolution ($\sim$ 1.2–2 times the nozzle diameter). Although the inkjet printhead is capable of printing at high printing frequencies (up to 30 kHz), it is recommended to deposit droplets at printing frequencies less than 500 Hz (due to inconsistent pressure within the print-head at high printing frequencies) [184]. As the nozzle diameter in most jetting-based printing systems is relatively small, it can only print ink with a narrow range of viscosities that range between 3 to 30 mPa.s [185].

Jetting-based bioprinting is one of the pioneering 3D printing technologies to facilitate cell deposition for the fabrication of 3D tissues or organs. The various jetting-based bioprinting techniques include inkjet-based bioprinting [186], laser-induced forward transfer (LIFT)/laser-assisted bioprinting [187], acoustic-based bioprinting [188], microvalve-based bioprinting [189–191], and electrohydrodynamic jet bioprinting (also known as bio-electrospraying) [192]. It has emerged as an important technique in the rapidly evolving landscape of biotechnology and regenerative medicine for manipulating, patterning, and assembling biologically relevant materials (cells, biomolecules, and biomaterials) in the form of ejected droplets to achieve specific biological functions in a DOD manner. Some important process considerations during jetting-based printing of tissue constructs include droplet impact velocity [193], bio-ink viscosity [194], shear stress [195], and cell homogeneity [196–198]. It was reported that the impact velocity of low-viscosity droplets (in the order of 1 mPa.s) has a significant effect on the cell viability and the cell damage increases exponentially with increasing droplet impact velocity as the shear stress increases strongly with droplet velocity. Furthermore, the study has also shown that a minimum droplet volume of 20 nL per spot helps to mitigate evaporation-induced cell damage [193]. Conversely, an increase in bio-ink viscosity from higher polymer concentration resulted in improved cell viability even at higher droplet impact velocities due to the additional cushioning effect (higher energy dissipation) for the encapsulated cells during droplet impact on the substrate surface [194]. Another work reported that even short-time exposure to high shear stress (>5 kPa) is detrimental to the cell viability and its long-term proliferation profile during the jetting process [195]. Another important consideration is the cell homogeneity within the bio-inks during the jetting-based printing process [196]. Over time, the suspended cells within the bio-inks would sediment and adhere to the interior surface of the printing cartridge which lead to cell inhomogeneity. It was reported that the use of polyvinylpyrrolidone-based bio-ink helped to reduce cell adhesion and mitigate sedimentation during the printing process [197], which improved cell homogeneity within the bio-inks. The different types of bio-inks used in jetting-based bioprinting include alginate-based (<2% w/v) [199–201], collagen-based (0.2%–0.3 w/v) [202–205], gelatin-based (up to 4% w/v) [206,207], and hyaluronic acid-based (up to 2.5% w/v) [208,209].

3.1.5. Binder jetting

Binder jetting is the 5th most used 3D printing technique (2.36%), and it is used for the fabrication of 3D printed medical devices such as maxillofacial prostheses [210,211], orthopedics implants [212–214] and surgical models [215,216]. The powder (polymers, metals, or ceramics—typical particle size of $\geq$ 30 μm) is the fundamental building unit in the binder jetting process and an ideal powder should have a uniform flow with negligible force between the particles [217] (Table 1). In the binder jetting process, a fresh layer of powdered material is spread into a layer and selectively joined into a pre-defined shape via selective deposition of organic liquid binder in a layer-by-layer manner to obtain the final "green" printed parts (generally brittle and highly-porous). Additional post-processing steps such as infiltration and/or sintering can be performed to enhance the mechanical properties after the removal of "green" printed parts. Some potential advantages of the binder jetting process include a wide range of powdered materials for the fabrication process, printing at room temperature and ambient air, no need for support structures, and a high fabrication rate, while the limitations include the need for post-processing steps (sintering and infiltration), potential distortion of printed parts during densification process, high surface roughness and lower printing resolution [218].

Some strategies to improve the powder flowability include the use of additives and/or powder coatings and dry powder [219,220]. The choice of a suitable binder is important during the binder jetting process; it should have a low printable viscosity, consistent droplet dispensing, and clean burn-out characteristics [221–223]. The binding process is highly sophisticated and

dynamic; the nature of binder-powder interaction differs drastically with the wetting characteristics, geometry, diameter, and density of the powdered material and this interaction controls the geometry accuracy, mechanical properties, and final surface roughness of the printed parts. The droplet impact and binder infiltration are the leading causes of printing defects; high droplet impact may cause ejection of the fine powders from their original position (ballistic ejection) [224] while slow binder infiltration leads to droplet coalescence on the powder-bed surface which interferes with powder spreading for subsequent layers [225]. Some strategies to overcome these challenges include the addition of chemical fixatives to enhance the cohesiveness of the powder bed, improvement of the wetting characteristics of powder materials [226], and reduction of the dispensed droplet diameter to increase the binder infiltration rate [227].

A series of post-processing steps (debinding and sintering) is performed on the green body (metal) upon removal from the unbound powder. The debinding process removes the binder from the final printed parts before the sintering cycle and it is critical to minimize the residual stress during the debinding process. The different debinding approaches include thermal debinding, catalytic debinding, solvent debinding, and wick debinding [228,229]. Next, sintering is performed to densify and strengthen the green parts via high-temperature heat treatment [230]. The sinterability of the particles is dependent on their particle size [231] and particle morphology [232]. Material shrinkage is a common problem during the sintering process and this problem can be solved by using multimodal powder sizes [233]. Additional post-processing methods can be performed to achieve near-to-full-density parts; these approaches are dependent on the type of porosity—closed or open. Hot isostatic pressing can be applied to significantly reduce or eliminate pores in printed parts with closed porosity [234], whereas the infiltration approach is a process of filling a porous part with a liquid via capillary wetting. Some of the common infiltrants include epoxy or cyanoacrylate for polymer parts [235] and bronze for metal parts [236].

3.1.6. DED

DED is the 2nd least commonly used 3D printing technique (0.88%), and it is mainly used for the fabrication of 3D printed medical devices such as orthopedics implants [237–240]. A broad range of metals and even ceramics can be utilized in the DED process; they include chromium, H13 tool steel, Inconel 625, stainless steels, titanium alloy and tungsten, etc [241] (Table 1). In the DED process, focused thermal energy (from lasers, electron beam (EB) [242], or plasma/electric arcs [243]) is used to melt the simultaneously deposited metallic material (powder or wire form) to create a pool of molten metal with an underlying heat-affected zone (HAZ) along the deposition path [244]. The relative movement of the build plate to the deposition head is controlled by a computer numerical control (CNC) and the layer-by-layer fabrication process is repeated to obtain the finished part. A shielding gas is required to mitigate the oxidation reactions during the printing process by creating an inert atmosphere and a carrier gas is required to transport the metallic material through the deposition head to the pool of molten metal. The build plate (substrate) used in the typical DED process has a similar material composition as the material preform and the finished part is removed from the substrate after the printing process. Thermal monitoring using infrared cameras and/or pyrometers in the DED process is useful for data collection and feedback control [244–246].

The key advantages of the DED process include the ability to fabricate functionally graded parts with different material/alloy concentrations and perform potential repair/cladding applications [247,248]. The preform used in the DED process can be in the form of powder or wire. Both the powder-fed and wire-fed DED processes have their unique advantages and limitations. The use of the powder-fed DED process is more predominant as the blown powder dynamics can be controlled in real-time and can be altered to achieve the fabrication of complex structures with higher precision [249,250]. Different methods such as gas atomization, water atomization, and plasma rotating electrode process (PREP) are typically used to produce the spherical powders (10–100 μm diameter) used in the DED process [251]. The use of spherical-shaped powders helps to minimize the amount of inert gas trapped within the melt pool and reduce the overall porosity of the finished part. In contrast, the wire-fed DED process resulted in improved surface quality and process efficiency, but it requires a higher degree of control due to potential vibrations [252].

Some key considerations during the DED process include using an optimal working distance [253] and thermal distortion [254,255]. The optimal working distance in the DED process is dependent on a few key parameters such as laser attenuation, distribution of powder concentration, heat, and mass transfer into the melt pool [253]. The DED printing process produces high-temperature gradients which lead to residual stresses and plastic deformations that affect the structural performance and metallurgy of the printed parts. Thermal distortion of DED printed parts is influenced by the preheating and cooling conditions, printing parameters, and the geometry of the printed part [256,257]. Particularly, depositing the first layer on a cold substrate during the DED process generates the most residual stresses due to high-temperature gradients, and reducing the substrate size can reduce the residual stresses due to lower heat flux and stiffness [255].

3.1.7. Sheet lamination

Sheet lamination is the least commonly used 3D printing technique (0.59%), and it has only been used for the fabrication of 3D-printed medical devices such as maxillofacial prostheses [258]. It can utilize a wide range of materials such as polymers, metals, ceramics, and even composites [259] (Table 1). In the sheet lamination process, sheets of material of pre-defined shape/geometry are bonded together to form the 3D finished parts. The layer thickness is dependent on the thickness of the sheets of materials, and it determines the final quality of the printed part. There are different bonding mechanisms for the sheet lamination process which include gluing/adhesive bonding, thermal bonding, clamping, and ultrasonic welding. The gluing/adhesive bonding approach requires the use of adhesive-backed material sheets that provide bonding between adjacent layers. The thermal bonding approach facilitates the bonding of adjacent layers by heating the material slightly above its melting point in an inert environment. The clamping approach requires a bolt and/or clamping mechanism to hold the sheets together; this approach results in clamping forces that are perpendicular to the laminate interface and there is a possibility of delamination. The ultrasonic welding approach applies ultrasonic wave and mechanical pressure on the material sheets to facilitate diffusion-based bonding [259]. The bonding/-forming order can be categorized as "bond then form" or "form then bond" processes and the advantages and limitations of both processes will be discussed in the following sections.

The "bond then form" approach comprises sheet alignment, sheet bonding and lastly forming process (cutting according to the slice contour). A heated roller is typically used to melt the adhesives and bond the adjacent sheet layers (70–200 μm thickness) and a laser/mechanical cutter is used to obtain the defined shape/geometry of each layer. The remaining material sheet provides support for subsequent layers and the process is repeated to obtain the 3D finished parts. The advantages of the "bond then form" sheet lamination process include low material shrinkage, high fabrication speed, multi-material fabrication, and relatively lower material, machine, and process cost, whereas the limitations

include the presence of glue leads to inhomogeneous mechanical and thermal properties, poor control over the dimensional accuracy due to inconsistent material sheet thickness and challenging to achieve small internal structures [260]. For the "form then bond" process, the defined shape/geometry is cut from the material sheet and then bonded with the preceding substrate until the 3D finished part is obtained. The "form then bond" process enables the fabrication of intricate features and channels, prevents cutting into previous layers, and eliminates the material removal step, but it requires an alignment system for accurate bonding between adjacent layers [260].

3.2. Build orientation and location

The build orientation and location of CAD models within the build volume of different additive manufacturing (AM) processes play a critical role in influencing the properties of printed parts. The build orientation is denoted by the *X*-, *Y*- and *Z*- axes (order of letters is based on decreasing dimensions—longest to shortest) and the build location refers to the spatial position of the parted parts within the build volume (Fig. 2(a)) [262].

Selecting an optimal build orientation for a given part can improve the quality of the final printed part [263–265]. Extensive studies were performed to determine the optimal build orientation and the optimization process leads to fewer support structures [266–271], improved surface roughness [266,268,271–273], reduced material cost [266,271,272], reduced build time [266,268,271], improved mechanical properties [266] and lastly higher printing accuracy [272]. The build orientation in FDM process (material extrusion AM process) influences the ductility and failure behavior of printed parts; the printed parts in on-edge (*XZY*) and flat (*XYZ*) orientation exhibited higher tensile strength, flexural strength, and stiffness as compared to parts printed in upright orientation (*ZXY*) [274]. Another study evaluated the influence of build orientation in the SLM process (powder bed fusion process); the printed Ti-6Al-4V parts in three different orientations (on-edge, flat, and up-right) showed similar α and prior-β grain sizes, similar elastic modulus regardless of its build orientation [275]. However, the change in build orientation influences the ductility of printed samples, with the flat-orientated samples showing the lowest elongation at break values. This is likely due to the curling of the flat-orientated samples which led to the generation of defects during the processing of successive layers [275]. Another study evaluated the tensile properties of PolyJet 3D printed parts (material jetting process) at different build orientations; the microstructure analysis showed that the direction of surface cracks/voids is dependent on the build orientation [276]. The influence of build orientation on built parts from vat polymerization showed that the samples built in the upright orientation had the highest fracture load values [277].

The mechanical properties of a printed part are directly affected by the build location; the variation in delivered energy at different locations (e.g., center vs edges) resulted in printed parts of different mechanical properties. A study that studied the influence of build position reported that the fabricated EBM parts showed finer microstructures at the top of the build part and coarser microstructures at the bottom of the build part [278]. Furthermore, it was reported that the fracture toughness of fabricated AM parts at different locations varies significantly (Fig. 2(b)) [279]. Hence, both build orientation and location play a critical part in influencing the mechanical properties of printed parts.

3.3. Support structures

The presence of support structures offers more freedom of design to fabricate highly complex geometries using 3D printing technologies [280]. The use of support structures is critical for the design and fabrication of complex structures; the number, type, and position of support structures used during the 3D printing process would affect the mechanical properties and geometric accuracy of the 3D printed parts [281]. It is interesting to note that the critical overhang angle varies among the different 3D printing processes such as material extrusion, powder bed fusion, and vat polymerization [281]. Automated algorithms are commonly used to determine the optimal number and position of supports to minimize material wastage and manual intervention may be required for more complex structures. Hence, it is important to analyze the geometry of printed parts (overhangs, high aspect ratio features, internal features, and thin features). Although the support structures can be removed via physical or chemical approaches, the removal process often leads to surface marks or residues.

A combination of optimized topology and build orientation for modified CAD models can help to minimize the required number of support structures [282–284]. The use of topology optimization in the FDM process has significantly reduced the number of support structures; numerical experiments are validated through the FDM process to demonstrate the robustness and efficiency of the proposed support structure-constrained topology optimization method [285]. Furthermore, a single-step optimization process can be implemented to simultaneously optimize the topology, build orientation, and support structures to minimize the number of support structures in the powder bed fusion process. High-quality solutions can be obtained using the proposed multi-optimization method (tested in a two-dimensional setting using a simplified support cost model) at a fraction of the time as compared to the fixed-orientation approaches [286]. A two-step optimization process was performed using the Matlab algorithm in another work to optimize the build orientation and cellular structures for minimal support structures [287]. Another study reported the use of lattice support structures with a low volume fraction of up to 8% for Ti6Al4V parts built using DMLS to reduce the amount of material and time used in the fabrication of support structures [288]. A similar study evaluated the influence of different lattice support structures on maximum normalized residual stresses in laser powder bed metal additive manufacturing; the diagonal lattice support structure demonstrated the most significant stress minimization (Fig. 3) [289] (See Table 2).

4. Material Considerations

4.1. Material batch-to-batch consistency

It is critical to determine the consistency of the raw materials and final 3D printed parts as the printing process might induce some chemical and/or physical changes to the material. A series of steps to ensure material consistency includes proper documentation of the material composition and evaluation tests for different AM techniques. Proper documentation of the printing material composition (raw material, additives, cross-linkers, or processing aids) includes recording the material supplier, material name, and its Chemical Abstracts Service (CAS) number, material specifications, and material certificates of analysis (COAs). Furthermore, it is also important to perform appropriate characterization and aging tests based on the material type (metal, ceramic, and polymer) and form (powders, filaments, fluid, and hydrogels) used in each specific AM technique over time. The characterization tests for different material types include the evaluation of chemical composition for metal, metal alloy, or ceramic materials and the evaluation of chemical composition, molecular weight distribution, and temperatures (glass transition (T_g), melting (T_m), and crystallization (T_c)) for polymers. The characterization tests for materials

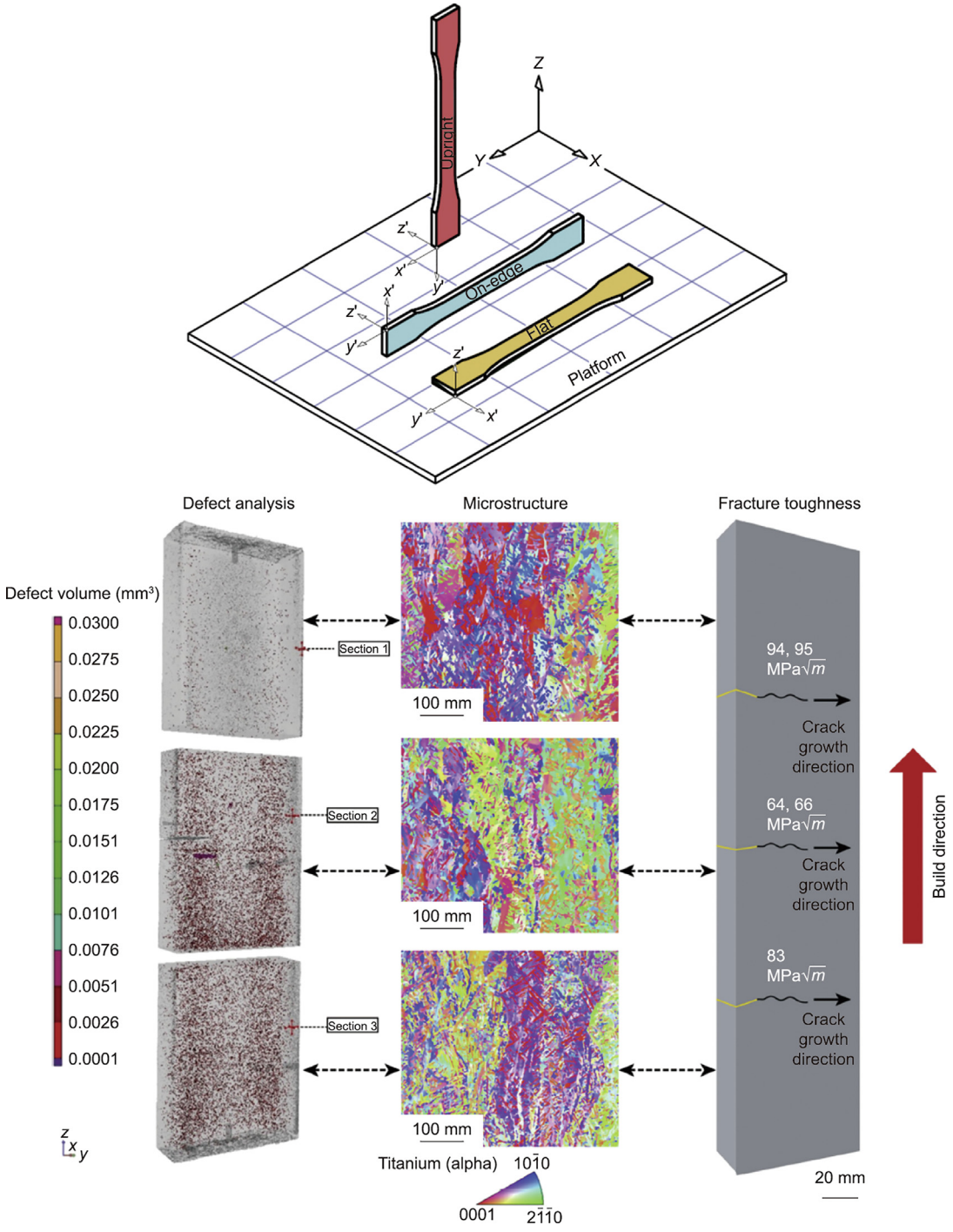

Fig. 2. (a) Different process parameters: various build orientations are denoted by *X*-, *Y*- and *Z*- axes (order of letters is based on decreasing dimensions—longest to shortest); upright (*ZXY*-red), on-edge (*XZY*-blue), and flat (*XYZ*-yellow). Reproduced from Ref. [274] with permission. (b) Location-dependent properties in as-deposited EBM Ti-6Al-4V materials are affected by convoluted interactions between defect-dominated and microstructure-dominated contributions. Reproduced from Ref. [279] with permission.

of the different forms include evaluation of powder diameter, powder size distribution and its rheological behavior, evaluation of filament diameter and its diametric tolerances, and evaluation of fluid viscosity or viscoelasticity and its pot life.

4.2. Material recycling

Material recycling in some of the 3D printing processes such as powders from binder jetting, DED, powder bed fusion processes, and resins from vat photopolymerization raised concerns over the possible alteration of material properties from its virgin state. The recycled free powder after a print may contain defects from elevated bed temperature and excessive sintering, whereas there might be partial polymerization of the resin during the photo-crosslinking process.

The recycled powders from the binder jetting process were stored and dried at 180 °C overnight in a vacuum to remove the moisture and passed through a 45 μm sieve. The presence of deformed powder particles was observed for unused stainless steel powders; the ratio of larger particles (>30 μm) to smaller particles

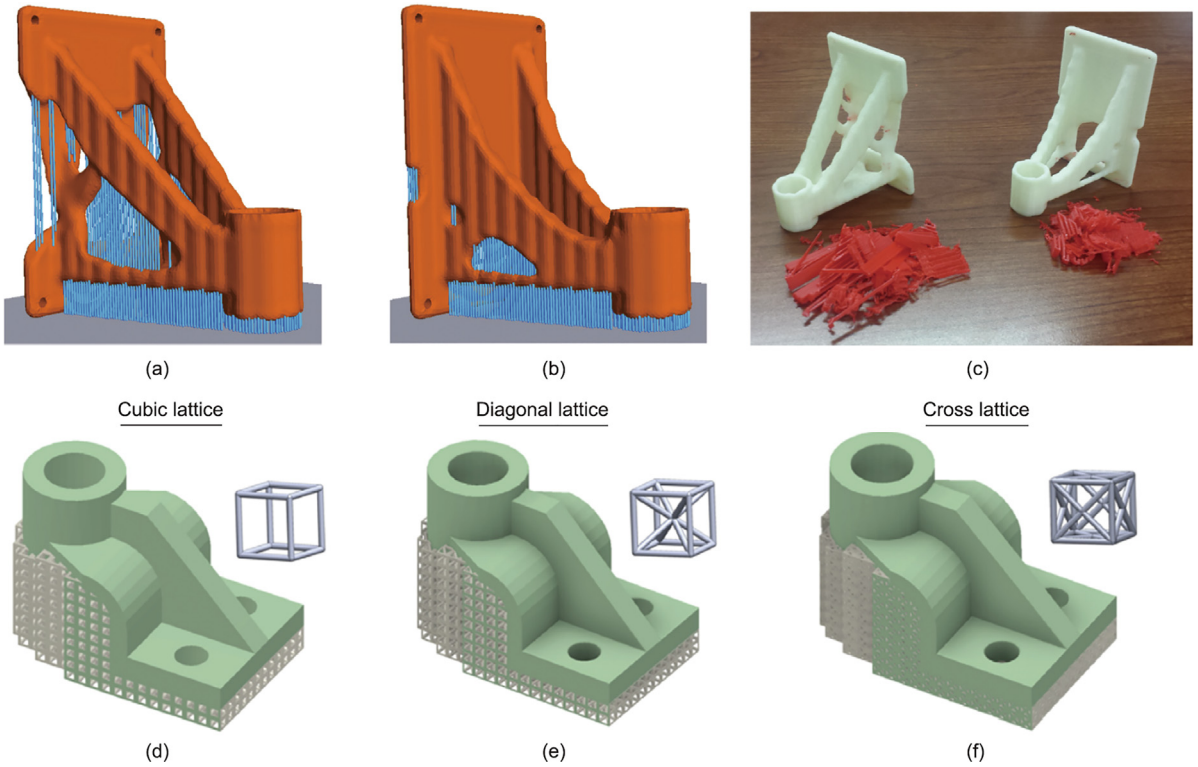

Fig. 3. Implementation of topology optimization to obtain designs with maximum performance and significantly reduced support structures using a support structure constraint methodology; optimized mount bracket at 0.7 volume fraction, (a) unconstrained, (b) relative constraint, η = 0.80, and (c) 3D printed mount bracket and their required support structures at 0.7 volume fraction (left: unconstrained design resulted in more support structures, right: constrained design with η = 0.80 resulted in less support structures). Reproduced from Ref. [285] with permission. (d) CAD model of bearing brackets with different lattice support structures (cubic, diagonal, and cross). (e) Comparison table of optimization results for the three different lattice support structures. Reproduced from Ref. [289] with permission.

Table 2
Comparison of the optimization results of the three lattice structure type.

	Cubic	Diagonal	Cross
Initially smallest maximum normalized stress	1.56	14.24	1.48
Optimized maximum normalized stress	1.06	0.93	1.16
Optimal orientation (Φ, φ)	(−2.359, 0.08)	(−2.343, 0.004)	(2.348, 0)
Support volume of optimal orientation (mm^3)	1.0212×10^4	3.288×10^4	3.007×10^4
Total iteration	54	50	37
Average computational cost per orientation (seconds)	—	20.9	—
Total computational cost (hours)	5.62	5.21	3.85

(<10 μm) increases after repeated recycling process (Fig. 4(a)) [290]. Interestingly, the final printed parts using both fresh and recycled powders exhibited comparable hardness and yield strength even though the density of sintered parts from fresh powder was ~1.5% higher than the recycled powder (Fig. 4(b)) [290].

Another study reported that the recycled titanium powders from the powder bed fusion EBM process showed an increased number of finer particles with a lower degree of fluidity, whereas the recycled nickel alloy powders for the powder bed fusion SLM process showed an increased number of coarse particles and higher fluidity [291]. Although similar microstructures were observed from both new and recycled SLM powders, an increased porosity in fabricated parts using recycled powders was observed. Comparable ultimate tensile strength and yield strength were observed for both new and recycled powders, while there was a decrease in the ductility and impact toughness for the recycled powders [291].

A recent study evaluated the influence of recycling on the zirconia-based slurry for vat photopolymerization; agglomeration of zirconia was observed (Fig. 4(c)) and it increased the slurry viscosity (Fig. 4(d)). Furthermore, there was a significant decrease in density of sintered parts from >99% in pristine samples to ~90% in recycled samples. Although the sintered parts from both samples showed similar hardness, there was a significant decrease in flexure strength (Fig. 4(e)) and Young's modulus (Fig. 4(f)) for the recycled samples. Hence, the ceramic-based slurry may not be suitable for material recycling in the vat photopolymerization 3D printing technique [292]. To date, there are only limited investigations on the suitability of recycled materials in different 3D printing processes and it is important to conduct a series of more extensive tests to carefully evaluate the suitability of material recycling for different 3D printing processes.

4.3. Protein adsorption on the material interface of printed parts

The protein adsorption on the material interface plays a critical role in regulating cell adhesion on the material interface. Protein adsorption at a material interface refers to the process by which proteins in a biological fluid bind onto the surface of a material. The key mechanism behind protein adsorption at the material

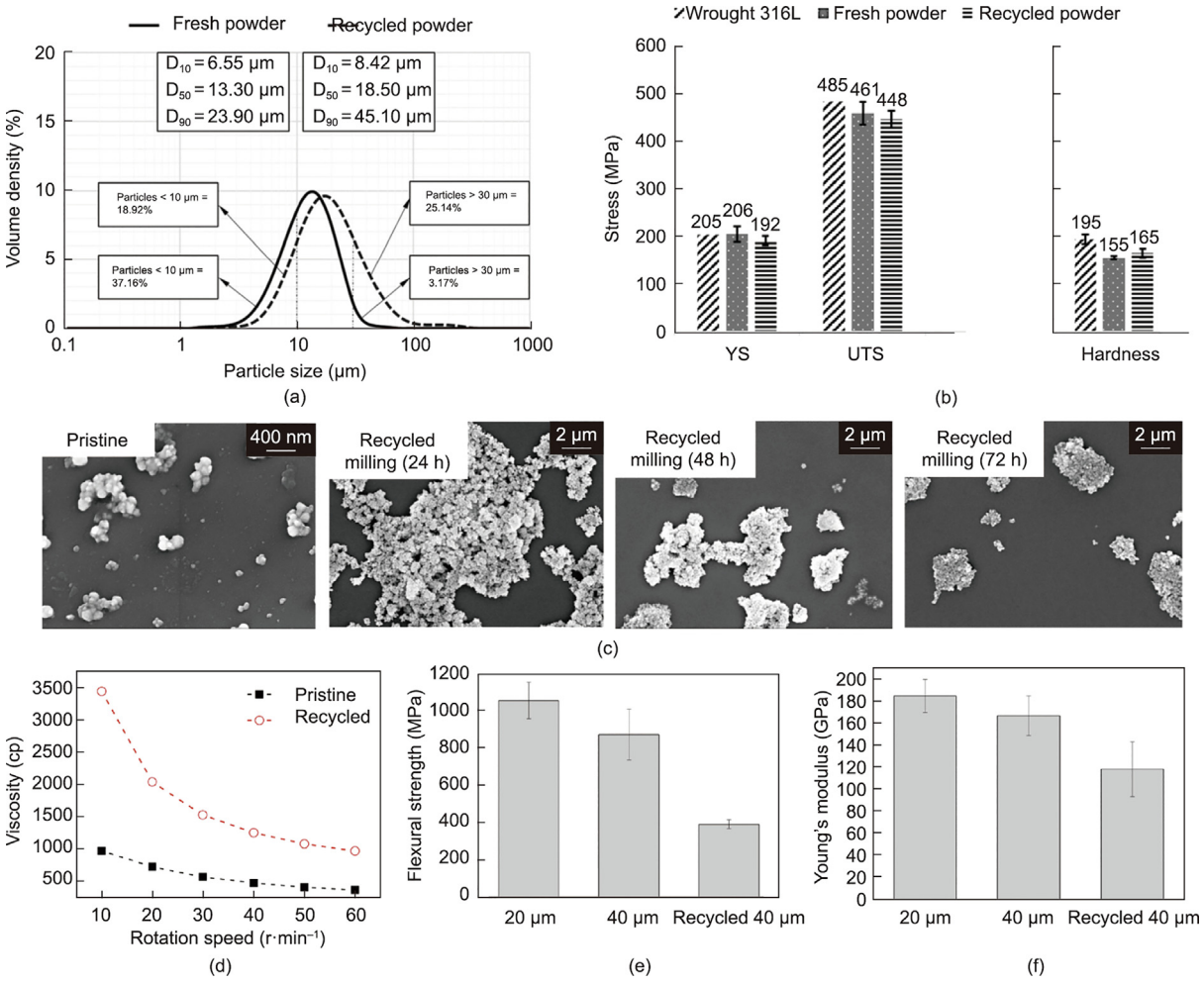

Fig. 4. (a) Influence of material recycling on the particle size distribution for stainless steel 316L obtained by laser diffraction technique (solid line: fresh powder, dotted line: recycled powder). (b) Mechanical properties of wrought 316L and 3D printed parts using binder jetting technique with fresh and recycled 316L powder. Reproduced from Ref. [290] with permission. (c) Representative images of pristine and recycled zirconia after milling for 24, 48, and 72 h, (d) Influence of pristine and recycled zirconia powder on the slurry viscosity at varying rotation speed. (e) Flexural strength and (f) Young's modulus of sintered zirconia parts printed at a layer thickness of 20 μm (pristine) and 40 μm (pristine and recycled). Reproduced from Ref. [292] with permission.

interface is due to the displacement of organized water molecules (lower entropy, higher free energy) by proteins [293]. The water molecules would influence the protein conformation and expose binding sites for interaction with the material interface; hence affecting the type and strength of interactions between the protein and material interface. Furthermore, the protein adsorption onto a material interface is also influenced by several other factors such as its protein structure (primary, secondary, tertiary, and quaternary) [294], isoelectric point [295], solubility [296], and wettability [297]. The free binding sites on the adsorbed protein layer can then facilitate cell adhesion and proliferation, which may be beneficial to tissue integration and wound healing [298]. In contrast, excessive protein adsorption can lead to material "fouling" which can impair the device's function and trigger adverse reactions in the body [299].

Different material surface properties such as surface chemistry, wettability, and topography can affect the protein adsorption and cell adhesion at the material interface (Fig. 5(a)) [300]. Substantial research works on surface chemistry aim to create uniformly coated material surfaces with different chemical functionalities that can prevent non-specific protein adsorption and provide bioinert surfaces. The surface chemistry plays a critical role in influencing the type, conformation, and strength of protein adsorption (Fig. 5(b)) [301–304]. The amount, type, and conformation of the adsorbed proteins (such as collagen, vitronectin, fibronectin, and laminin) regulate integrin binding, which can trigger different signaling pathways that control various cellular functions. The cells begin to spread and stretch on the surface after adhering to the surface; the protein-mediated adhesive interactions serve as mechano-sensors that facilitate cell-ECM interactions [305,306]. The most common strategy to functionalize the material surface is to apply various monolayer/multilayer polymer coatings [307]. Although this method is effective in reducing protein adsorption and thrombocyte activation, some of the existing challenges include the development of homogeneous and long-term stable monolayer coatings on chemically inert surfaces [308]. Surface wettability can be referred to as hydrophobicity/hydrophilicity and it is an important factor that affects protein adsorption. It is well-documented that protein unfolding and surface coverage are significantly higher on hydrophobic surfaces than on hydrophilic surfaces [309]. The proteins are shielded from the hydrophilic surface due to the strong water-surface interactions on hydrophilic surfaces and are consequently desorbed. Lastly, the surface topography of a device can be manipulated to control cell adhesion via protein adsorption. The different surface topographical cues including surface roughness, curvature and size of surface features can induce changes in the protein's structure and orientation which affect the cell adhesion at the material interface [310,311].

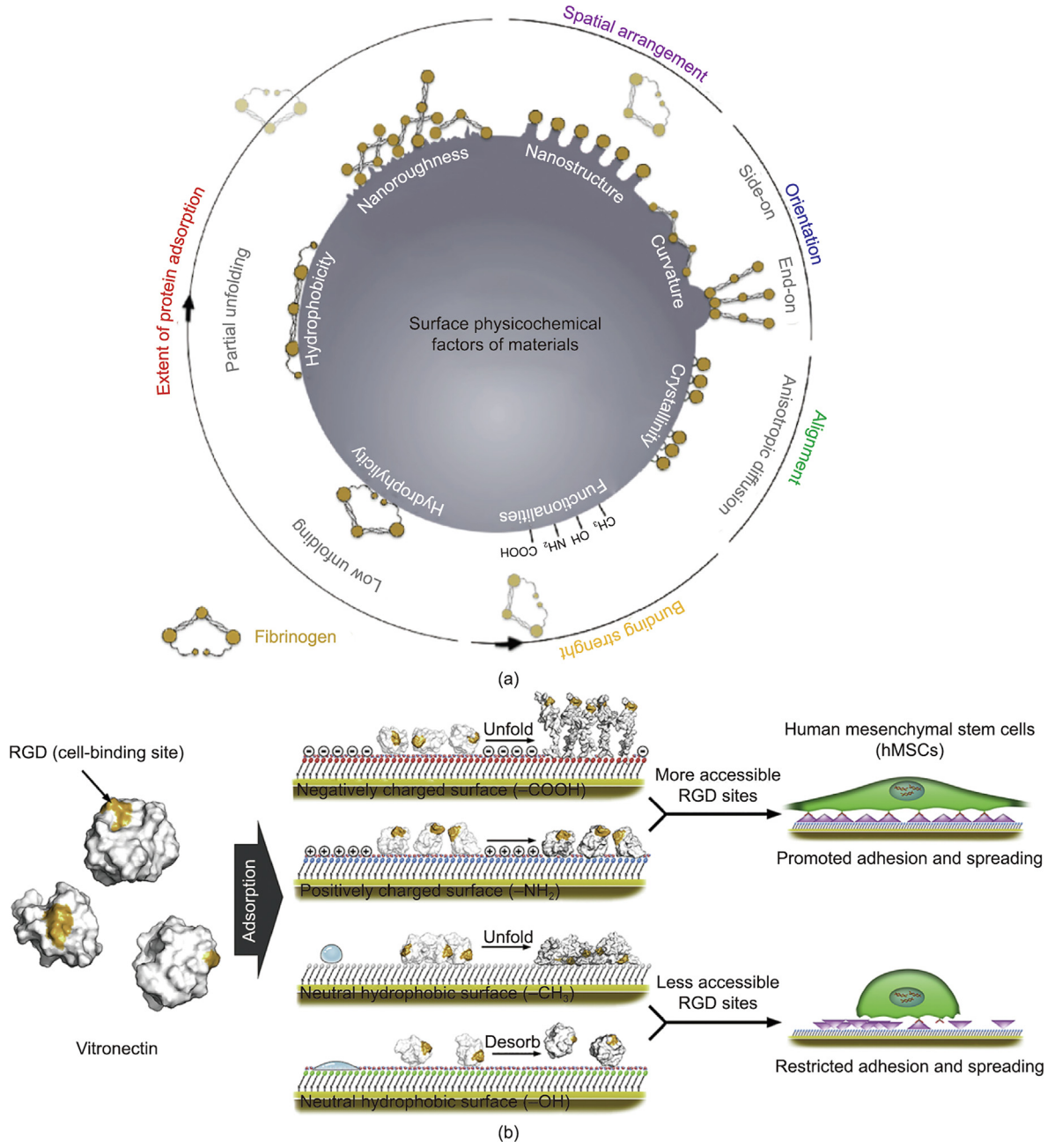

Fig. 5. (a) Influence of material surface properties (surface chemistry, wettability, and topography) on protein adsorption behavior, such as, the extent and binding strength of protein adsorption, alignment, orientation, and spatial arrangement of proteins. Reproduced from Ref. [300] with permission. (b) Schematic drawing to illustrate the underlying mechanisms for vitronectin adsorption on different self-assembled monolayers (SAMs) with four kinds of terminal groups (—COOH, —NH_2, —CH_3, and —OH) to serve as model surfaces with opposing charges or wettability. The arginyl-glycyl-aspartic acid (RGD) loops were unrestrained and accessible for cell binding on both negatively and positively charged surfaces, whereas most of the RGD loops were restrained by substrates and deactivated for integrin binding on neutral hydrophobic surfaces or the vitronectin proteins are shielded and consequently desorbed from neutral hydrophilic surface. Reproduced from Ref. [304] with permission.

A high-throughput and quantitative approach was implemented to investigate the influence of surface roughness, protein concentration, and protein type on the protein-surface interactions [312]. The surface roughness has a significant effect on the adsorbed proteins; the study showed that an increase in surface roughness (from 15 to 30 nm) resulted in a significant increase in saturation uptake (up to 600%). Furthermore, the nanostructured surfaces were shown to promote the formation of protein aggregates within the nanometric pores with an aspect ratio greater than 0.4 (depending on the characteristics of each protein) [312]. Another critical parameter for surface topography is surface curvature; different studies have reported that an increase in the local curvature would lead to decreased protein adsorption [313,314]. Hence, a good understanding of the material surface properties is important for the development of advanced biomaterials to manipulate protein adsorption and regulate cell adhesion on material interfaces.

4.4. Biocompatibility of printed parts

A biocompatible material does not induce any adverse reaction when in contact with surrounding living tissues [315]. The different factors that influence the biocompatibility of a printed product include the chemical composition [316] and surface properties

[317]. The final finished products may undergo a range of post-processing procedures which can lead to a significant change in the surface chemistry and topography which in turn affects the biocompatibility [317]. It is recommended to test the medical devices in their final finished form and composition after the various post-processing steps (sintering, coating, cleaning, and sterilization).

The establishment of ISO 10993-5 aims to standardize various existing procedures and specifies the requirements and guidelines for the *in-vitro* cytotoxicity testing of devices [318]. The goal of *in-vitro* cytotoxicity testing is to evaluate the potential of a device to cause cell damage and ensure its safety for use in humans. ISO 10993-5 protocol involves the use of established cell lines (ATCC CCL-1, CCL-10, CCL-75, CCL-81, CCL-163, and CCL-171 endorsed by ISO experts) for preliminary phase of investigation, which includes accurate and reproducible quantitative measurement of cell metabolic functions, via cell-counting procedures [319], DNA level assessment [320] and MTT assay [321].

4.5. Degradation properties of 3D printed parts

Most medical devices are fabricated using biocompatible materials (metals, ceramics, or polymers) and these materials are likely to produce harmless degradation by-products as the implanted medical devices degrade over time within the human body. It is important to note that the degradation profiles of metal-based, ceramic-based, or polymer-based medical devices can vary significantly. Metals and ceramics are highly resistant to corrosion and degradation under physiologic conditions, making them durable for long-term implantation [322–324]. In contrast, the polymers undergo different forms of degradation such as hydrolysis, oxidation, and mechanical wear [325,326]. Although there are strategies to minimize/isolate the release of degradation by-products from implanted medical devices to surrounding tissues via the use of medical coatings [327,328], the human body has the innate ability to metabolize and remove some of these degradation by-products [329]. Hence, the choice of suitable material for a specific medical device should depend on important factors such as intended application, biomechanical requirements, and the device's expected lifespan.

5. Regulatory considerations

3D printing technology has gained significant traction in the field of medicine and healthcare; different regulatory bodies around the world such as the Food and Drug Administration (FDA) from the United States, the European Medicines Agency (EMA) from the European Union, and National Medicine Products Administration (NMPA) from China have been actively involved in the regulation and approval of 3D printed medical devices. Some of the important milestones for FDA-approved 3D printing technology include the first FDA-approved 3D printed cranial implant (OsteoFab Patient-Specific Cranial Device received FDA clearance in February 2013) developed by Oxford Performance Materials (USA) and the first 3D printed titanium-based spinal device (CASCADIA Lateral Interbody System received its FDA 510(k) clearance and CE mark in January 2016) developed by K2M Group Holdings (acquired by Stryker in year 2018). To date, numerous 3D printing companies have received FDA 510(k) clearance for their 3D printed medical devices based on the findings published by the FDA department (Fig. 6). Since then, several studies demonstrated the

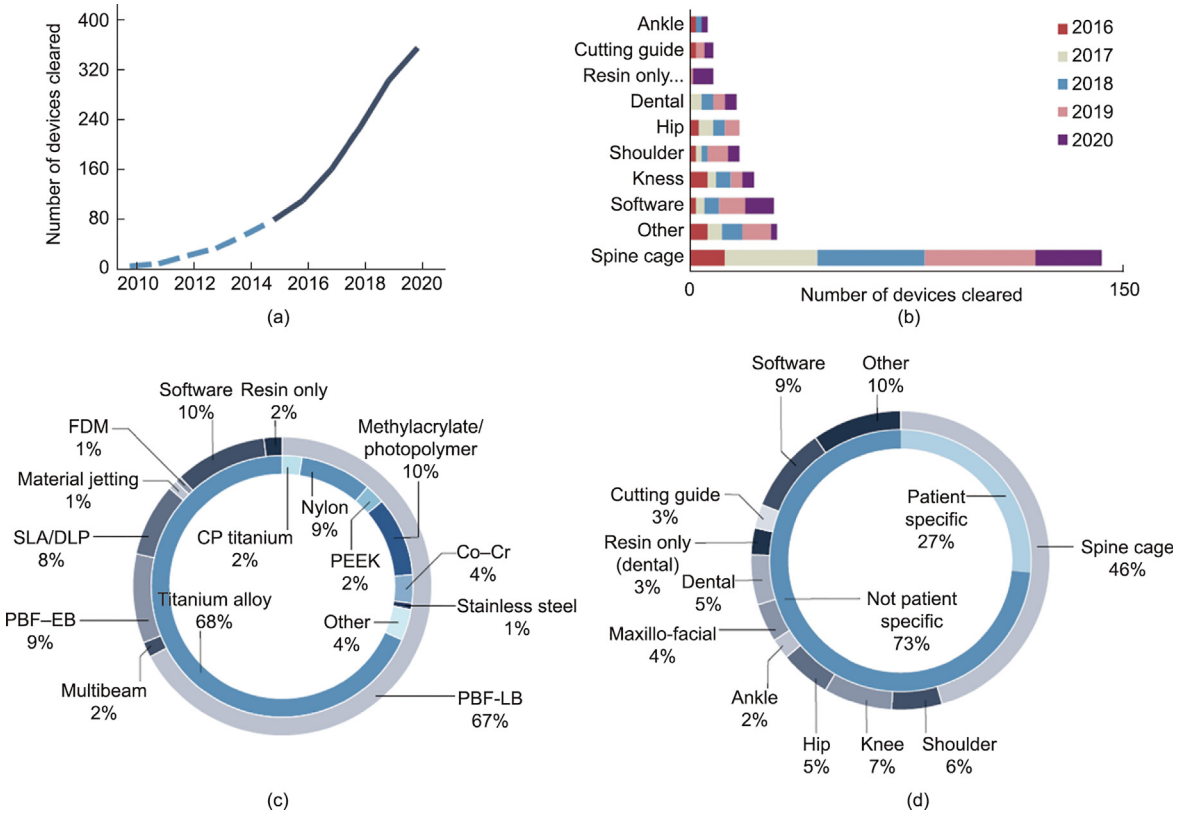

Fig. 6. FDA 510(k)-approved 3D printed medical devices. (a) Timeline of FDA-approved 3D printed medical devices from 2010 to 2020. (b) A detailed analysis of device type cleared within each year from the year 2016 to the year 2020. (c) Concentric pie chart indicating the printing technologies and materials. (d) Concentric pie chart indicating the device type and patient specificity. The data set above only contains 3D-printed medical devices that were declared substantially equivalent through the FDA's 510(k) pathway and does not include 3D-printed medical devices cleared through other pathways. Reproduced from Ref.[335] with premission.

implementation of 3D-printed medical devices into human bodies [330–333].

Despite the significant progress in the regulation of 3D printed medical devices, there are currently no FDA-approved or cleared 3D bioprinted tissues/organs. To date, there is a lack of standardization in the field of 3D bioprinting (in terms of technology, materials, and process), which severely limits its adoption for clinical medicine. Furthermore, the 3D bioprinted cell-laden tissues/organs pose several challenges to regulatory authorities due to their increased complexity as compared to conventional 3D printed medical devices. Although good practices such as documentation of the cell source, evaluation of cell viability and function, and maintenance of a high standard of sterility can be adopted during the entire bioprinting process, some of the remaining bottlenecks include the logistics and unknown long-term safety in human hosts. There are limited research facilities that have the expertise and technology to fabricate 3D bioprinted tissues/organs; hence the patient-derived cells and extracellular matrices would need to be transported to a specialized biofabrication facility for tissue/organ fabrication and maturation before sending the matured tissue/organ back to the clinical facilities. The logistics can be highly challenging as transportation of living tissues/organs is a highly specialized and time-sensitive process that requires careful coordination and adherence to strict protocols to ensure that the 3D bioprinted tissues/organs remain viable and safe for transplant. Nevertheless, a recent study has offered some glimpse of hope in a first-of-its-kind clinical trial—the first transplantation of autologous bioprinted ear implant in humans (developed by 3D Bio Therapeutics) was demonstrated in June 2022, which highlighted the potential of 3D bioprinting technology for translational medicine [334].

Although there is currently no FDA-approved 3D bioprinted tissue construct, numerous 3D printing companies have received FDA 510(k) clearance for their 3D printed medical devices. Some important regulatory considerations of 3D-printed medical devices include sterility and mechanical properties of printed parts. It is important to adhere to the strict guidelines and requirements for the sterility of medical devices to mitigate the potential occurrence of infections. Furthermore, many medical devices (orthopedic implants, prostheses, and surgical instruments) require specific mechanical properties to perform their intended functions effectively and mechanical failures can lead to serious consequences during use. In the subsequent sections, more detailed discussions ofthese key areas will be provided.

5.1. Sterility of printed parts

A sterile implant reduces the risk of potential infections and ensures the safety and effectiveness of the implantation process [336,337]. Sterility refers to the absence of pathogenic microorganisms and it can be achieved through the use of different physical/-chemical sterilization methods such as heat [338], radiation [339], and chemicals [340–342]. The sterility assurance level (SAL) is a measure of the probability that a medical device is sterile and the accepted SAL for medical devices is 10^{-6} (one in a million chance).

The autoclaving process is a heat sterilization process that generates steam under pressure to eliminate microorganisms. The effectiveness of the autoclaving process in eliminating microbes is dependent on the temperature, the contact duration, and the free circulation of pressurized steam [338]. However, the autoclaving sterilization method is not suitable for devices that are sensitive to heat or moisture. Gamma radiation is a type of ionizing radiation that can destroy microorganisms by destroying their DNA. Although it is an effective sterilization for devices that are sensitive to heat and chemicals, the high-energy gamma radiation can damage the polymer molecules over time and affect their chemical and physical properties. Chemical sterilization uses chemicals such as hydrogen peroxide (H_2O_2) [340], ethylene oxide (C_2H_4O) [341], or glutaraldehyde [342] to kill the microorganisms. The chemical sterilization process involves exposing the devices to the chemicals at controlled temperature, humidity, and duration for effective sterilization. Although it can be used to sterilize devices that are sensitive to heat and radiation, some of the chemicals may be toxic and additional steps are required to remove the residual chemicals on the devices. Hence, the selection of suitable sterilization techniques is dependent on the material properties of the printed devices. Notably, the FDA recently approved the first H_2O_2 sterilization system from Steris Healthcare (Ireland) in August 2023 for the sterilization of 3D-printed medical devices.

5.2. Mechanical properties of printed parts

A critical aspect of medical device testing considerations includes mechanical testing for patient-specific AM parts [343]. Upon completion of different post-processing, cleaning, and sterilization steps, the final finished AM parts should be subjected to similar mechanical testing as those fabricated using conventional manufacturing methods (tensile, compression, bend, fatigue, impact tests, etc). The final finished parts or representative test coupons should be used for recommended testing and more emphasis should be placed on structures containing voids, supports, or porous regions. The device type and application determine the type of tests to be conducted (such as ultimate strength, yield strength, modulus, creep, fatigue, and abrasive tests). Furthermore, it is important to perform proper documentation of all the post-processing steps (removal of residuals, heat treatment, and final machining) as the material properties and performance of final finished parts are affected by the post-processing steps [344,345]. As highlighted in an earlier section, the build orientation and location have significant effects on the properties of printed parts. Hence, it is important to develop a stringent manufacturing process with thorough monitoring to ensure the batch-to-batch consistency of final finished parts.

6. Concluding Remarks

3D printing has attracted increasing attention for the fabrication of medical devices and tissue constructs in recent years. There are seven classifications of 3D printing processes, and a good understanding of the different 3D printing processes, along with their advantages and limitations, is important for the selection of a suitable fabrication technique based on the intended application. Next, biomaterials play a critical role in the mechanical and biological properties of the 3D printed parts. Some of the critical material considerations include the consistency of batch-to-batch raw biomaterials, the effect of material recycling on the material properties, the influence of material surface properties on protein adsorption and cell adhesion at the material interface, biocompatibility and degradation properties of 3D printed parts. Lastly, the 3D-printed medical devices and tissue constructs should be subjected to stringent regulations in terms of sterility and mechanical properties to ensure their safety and efficacy. Hence, it is timely to provide a concise review that highlights the various important considerations (process, material, and regulatory) for 3D printed medical devices and tissue constructs. We envisioned that a good understanding of the various key considerations in 3D printing (process, material, and regulatory) is critical for the fabrication of improved patient-specific 3D printed medical devices and tissue constructs.

Declaration of competing interest

The authors declare that they have no known competing financial interests or personal relationships that could have appeared to influence the work reported in this paper.

Acknowledgments

Wei Long Ng acknowledges the support provided by the NTU Presidential Postdoctoral Fellowship.

Disclosure statement

Wei Long Ng, Jia An, and Chee Kai Chua declare that they have no conflict of interest or financial conflicts to disclose.

References

[1] Di Prima M, Coburn J, Hwang D, Kelly J, Khairuzzaman A, Ricles L. Additively manufactured medical products–the FDA perspective. 3D Print Med 2016;2:1–6.
[2] Zhang Y, Xia J, Zhang J, Mao J, Chen H, Lin H, et al. Validity of a soft and flexible 3D-printed Nissen fundoplication model in surgical training. Int J Bioprint 2022;8(2):546.
[3] Borràs-Novell C, Causapié MG, Murcia M, Djian D, García-Algar Ó. Development of a 3D individualized mask for neonatal non-invasive ventilation. Int J Bioprint 2022;8(2):516.
[4] Kang HW, Lee SJ, Ko IK, Kengla C, Yoo JJ, Atala A. A 3D bioprinting system to produce human-scale tissue constructs with structural integrity. Nat Biotechnol 2016;34(3):312–39.
[5] Ng WL, Chua CK, Shen YF. Print me an organ! Why we are not there yet. Prog Polym Sci 2019;97:101145.
[6] Kathawala MH, Ng WL, Liu D, Naing MW, Yeong WY, Spiller KL, et al. Healing of chronic wounds: an update of recent developments and future possibilities. Tissue Eng Part B Rev 2019;25(5):429–44.
[7] Ng WL, Chan A, Ong YS, Chua CK. Deep learning for fabrication and maturation of 3D bioprinted tissues and organs. Virtual Phys Prototyp 2020;15(3):340–58.
[8] Lee JM, Ng WL, Yeong WY. Resolution and shape in bioprinting: strategizing towards complex tissue and organ printing. Appl Phys Rev 2019;6(1):011307.
[9] Markets M. 3D printing medical devices market by component (3D printer, 3D bioprinter, material, software, service), technology (EBM, DMLS, SLS, SLA, DLP, Polyjet), application (surgical guides, prosthetics, implants), End user & region-global forecast to 2028. Report. USA: 3D Printing Medical Devices Market. 2023.
[10] Santoni S, Gugliandolo SG, Sponchioni M, Moscatelli D, Colosimo BM. 3D bioprinting: current status and trends—a guide to the literature and industrial practice. Biodes Manuf 2022;5(1):14–42.
[11] Honigmann P, Sharma N, Schumacher R, Rueegg J, Haefeli M, Thieringer F. In-hospital 3D printed scaphoid prosthesis using medical-grade polyetheretherketone (PEEK) biomaterial. BioMed Res Int 2021;2021:1301028.
[12] Cuellar JS, Plettenburg D, Zadpoor AA, Breedveld P, Smit G. Design of a 3D-printed hand prosthesis featuring articulated bio-inspired fingers. Proc Inst Mech Eng H 2021;235(3):336–45.
[13] Fay CD, Jeiranikhameneh A, Sayyar S, Talebian S, Nagle A, Cheng K, et al. Development of a customised 3D printer as a potential tool for direct printing of patient-specific facial prosthesis. Int J Adv Manuf Technol 2022;120(11–12):7143–55.
[14] Rodriguez Colon R, Nayak VV, Parente PEL, Leucht P, Tovar N, Lin CC, et al. The presence of 3D printing in orthopedics: a clinical and material review. J Orthop Res 2023;41(3):601–13.
[15] Petersmann S, Smith JA, Schäfer U, Arbeiter F. Material extrusion-based additive manufacturing of polyetheretherketone cranial implants: mechanical performance and print quality. J Mater Res Technol 2023;22:642–57.
[16] Jeyachandran P, Bontha S, Bodhak S, Balla VK, Doddamani M. Material extrusion additive manufacturing of bioactive glass/high density polyethylene composites. Compos Sci Technol 2021;213:108966.
[17] Juneja M, Thakur N, Kumar D, Gupta A, Bajwa B, Jindal P. Accuracy in dental surgical guide fabrication using different 3-D printing techniques. Addit Manuf 2018;22:243–55.
[18] Rothlauf S, Pieralli S, Wesemann C, Burkhardt F, Vach K, Kernen F, et al. Influence of planning software and template design on the accuracy of static computer assisted implant surgery performed using guides fabricated with material extrusion technology: an in vitro study. J Dent 2023;132:104482.
[19] Burkhardt F, Spies BC, Wesemann C, Schirmeister CG, Licht EH, Beuer F, et al. Cytotoxicity of polymers intended for the extrusion-based additive manufacturing of surgical guides. Sci Rep 2022;12(1):7391.
[20] Higgins M, Leung S, Radacsi N. 3D printing surgical phantoms and their role in the visualization of medical procedures. Ann 3D Print Med 2022;6:100057.
[21] Turek P, Budzik G. Estimating the accuracy of mandible anatomical models manufactured using material extrusion methods. Polymers 2021;13(14):2271.
[22] Ravi P, Chepelev LL, Stichweh GV, Jones BS, Rybicki FJ. Medical 3D printing dimensional accuracy for multi-pathological anatomical models 3D printed using material extrusion. J Digit Imaging 2022;35(3):613–22.
[23] Skrzypczak NG, Tanikella NG, Pearce JM. Open source high-temperature RepRap for 3-D printing heat-sterilizable PPE and other applications. HardwareX 2020;8:e00130.
[24] Tarfaoui M, Nachtane M, Goda I, Qureshi Y, Benyahia H. 3D printing to support the shortage in personal protective equipment caused by COVID-19 pandemic. Materials 2020;13(15):3339.
[25] Leucht A, Volz AC, Rogal J, Borchers K, Kluger PJ. Advanced gelatin-based vascularization bioinks for extrusion-based bioprinting of vascularized bone equivalents. Sci Rep 2020;10(1):5330.
[26] Pant S, Subramanian S, Thomas S, Loganathan S, Valapa RB. Tailoring of mesoporous bioactive glass composite scaffold via thermal extrusion based 3D bioprinting and scrutiny on bone tissue engineering characteristics. Microporous Mesoporous Mater 2022;341:112104.
[27] Zhu H, Monavari M, Zheng K, Distler T, Ouyang L, Heid S, et al. 3D bioprinting of multifunctional dynamic nanocomposite bioinks incorporating cu-doped mesoporous bioactive glass nanoparticles for bone tissue engineering. Small 2022;18(12):2104996.
[28] Ratheesh G, Vaquette C, Xiao Y. Patient-specific bone particles bioprinting for bone tissue engineering. Adv Healthc Mater 2020;9(23):2001323.
[29] Lee A, Hudson AR, Shiwarski DJ, Tashman JW, Hinton TJ, Yerneni S, et al. 3D bioprinting of collagen to rebuild components of the human heart. Science 2019;365(6452):482–7.
[30] Mirdamadi E, Tashman JW, Shiwarski DJ, Palchesko RN, Feinberg AW. FRESH 3D bioprinting a full-size model of the human heart. ACS Biomater Sci Eng 2020;6(11):6453–9.
[31] Noor N, Shapira A, Edri R, Gal I, Wertheim L, Dvir T. 3D printing of personalized thick and perfusable cardiac patches and hearts. Adv Sci 2019;6(11):1900344.
[32] Bejleri D, Streeter BW, Nachlas ALY, Brown ME, Gaetani R, Christman KL, et al. A bioprinted cardiac patch composed of cardiac-specific extracellular matrix and progenitor cells for heart repair. Adv Healthc Mater 2018;7(23):1800672.
[33] Flégeau K, Puiggali-Jou A, Zenobi-Wong M. Cartilage tissue engineering by extrusion bioprinting utilizing porous hyaluronic acid microgel bioinks. Biofabrication 2022;14(3):034105.
[34] Beketov EE, Isaeva EV, Yakovleva ND, Demyashkin GA, Arguchinskaya NV, Kisel AA, et al. Bioprinting of cartilage with bioink based on high-concentration collagen and chondrocytes. Int J Mol Sci 2021;22(21):11351.
[35] Trachsel L, Johnbosco C, Lang T, Benetti EM, Zenobi-Wong M. Double-network hydrogels including enzymatically crosslinked poly-(2-alkyl-2-oxazoline) s for 3D bioprinting of cartilage-engineering constructs. Biomacromolecules 2019;20(12):4502–11.
[36] Ng WL, Lee JM, Zhou M, Yeong WY. Hydrogels for 3-D bioprinting-based tissue engineering. In: Narayan R, editor. Rapid prototyping of biomaterials. Cambridge: Woodhead Publishing; 2020. p. 183–204.
[37] Osidak EO, Kozhukhov VI, Osidak MS, Domogatsky SP. Collagen as bioink for bioprinting: a comprehensive review. Int J Bioprint 2020;6(3):270.
[38] Yang Y, Xu R, Wang C, Guo Y, Sun W, Ouyang L. Recombinant human collagen-based bioinks for the 3D bioprinting of full-thickness human skin equivalent. Int J Bioprint 2022;8(4):611.
[39] Liu S, Zhang H, Ahlfeld T, Kilian D, Liu Y, Gelinsky M, et al. Evaluation of different crosslinking methods in altering the properties of extrusion-printed chitosan-based multi-material hydrogel composites. Biodes Manuf 2023;6(2):150–73.
[40] Ng WL, Yeong WY, Naing MW. Potential of bioprinted films for skin tissue engineering. In: Proceedings of the 1st International Conference on Progress in Additive Manufacturing; 2014 May 26–28; Singapore. Hoboken: Research Publishing; 2014. p. 441–6.
[41] Goh G, Yap Y, Tan H, Sing S, Goh G, Yeong W. Process–structure–properties in polymer additive manufacturing via material extrusion: a review. Crit Rev Solid State Mater Sci 2020;45(2):113–33.
[42] Gibson MA, Mykulowycz NM, Shim J, Fontana R, Schmitt P, Roberts A, et al. 3D printing metals like thermoplastics: fused filament fabrication of metallic glasses. Mater Today 2018;21(7):697–702.
[43] Sarraf M, Rezvani Ghomi E, Alipour S, Ramakrishna S, Liana SN. A state-of-the-art review of the fabrication and characteristics of titanium and its alloys for biomedical applications. Biodes Manuf 2022;5(2):371–95.
[44] Yu T, Zhang Z, Liu Q, Kuliiev R, Orlovskaya N, Wu D. Extrusion-based additive manufacturing of yttria-partially-stabilized zirconia ceramics. Ceram Int 2020;46(4):5020–7.

[45] Zou A, Liang H, Jiao C, Ge M, Yi X, Yang Y, et al. Fabrication and properties of $CaSiO_3/Sr_3(PO_4)_2$ composite scaffold based on extrusion deposition. Ceram Int 2021;47(4):4783–92.
[46] Masood SH. Advances in fused deposition modeling. In: Hashmi S, Ferreira Batalha G, Van Tyne CJ, Yilbas B, editors. Comprehensive materials processing. Amsterdam: Elsevier; 2014. p. 69–91.
[47] Huang J, Chen Q, Jiang H, Zou B, Li L, Liu J, et al. A survey of design methods for material extrusion polymer 3D printing. Virtual Phys Prototyp 2020;15(2):148–62.
[48] Tamburrino F, Graziosi S, Bordegoni M. The influence of slicing parameters on the multi-material adhesion mechanisms of FDM printed parts: an exploratory study. Virtual Phys Prototyp 2019;14(4):316–32.
[49] Lewis JA. Direct ink writing of 3D functional materials. Adv Funct Mater 2006;16(17):2193–204.
[50] Brown TD, Dalton PD, Hutmacher DW. Direct writing by way of melt electrospinning. Adv Mater 2011;23(47):5651–7.
[51] Ng WL, Yeong WY, Naing MW. Polyelectrolyte gelatin-chitosan hydrogel optimized for 3D bioprinting in skin tissue engineering. Int J Bioprint 2016;2(1):53–62.
[52] Zhuang P, Ng WL, An J, Chua CK, Tan LP. Layer-by-layer ultraviolet assisted extrusion-based (UAE) bioprinting of hydrogel constructs with high aspect ratio for soft tissue engineering applications. PLoS One 2019;14(6):0216776.
[53] Coogan TJ, Kazmer DO. Bond and part strength in fused deposition modeling. Rapid Prototyp J 2017;23(2):414–22.
[54] KJ, Chandrasekhar U, Venkateswarlu K. A study on the influence of process parameters on the mechanical properties of 3D printed ABS composite. In: IOP conference series: materials science and engineering. Bristol: IOP Publishing; 2016. p. 012109.
[55] Yin J, Lu C, Fu J, Huang Y, Zheng Y. Interfacial bonding during multi-material fused deposition modeling (FDM) process due to inter-molecular diffusion. Mater Des 2018;150:104–12.
[56] Lyu J, Manoochehri S. Online convolutional neural network-based anomaly detection and quality control for fused filament fabrication process. Virtual Phys Prototyp 2021;16(2):160–77.
[57] Suzuki M, Wilkie CA. The thermal degradation of acrylonitrile-butadiene-styrene terpolymei as studied by TGA/FTIR. Polym Degrad Stabil 1995;47(2):217–21.
[58] Davis CS, Hillgartner KE, Han SH, Seppala JE. Mechanical strength of welding zones produced by material extrusion additive manufacturing. Addit Manuf 2017;16:162–6.
[59] D'Amico AA, Debaie A, Peterson AM. Effect of layer thickness on irreversible thermal expansion and interlayer strength in fused deposition modeling. Rapid Prototyp J 2017;23(5):943–53.
[60] Carneiro OS, Silva A, Gomes R. Fused deposition modeling with polypropylene. Mater Des 2015;83:768–76.
[61] Braconnier DJ, Jensen RE, Peterson AM. Processing parameter correlations in material extrusion additive manufacturing. Addit Manuf 2020;31:100924.
[62] Gregorian A, Elliott B, Navarro R, Ochoa F, Singh H, Monge E, et al. Accuracy improvement in rapid prototyping machine (FDM-1650). In: Proceedings of the 2001 International Solid Freeform Fabrication Symposium; 2001 Aug 6–8; Austin, TX, USA. Austin: The University of Texas at Austin; 2001. p. 77–84.
[63] Pennington R, Hoekstra N, Newcomer J. Significant factors in the dimensional accuracy of fused deposition modelling. Proc Inst Mech Eng 2005;219(1):89–92.
[64] Anitha R, Arunachalam S, Radhakrishnan P. Critical parameters influencing the quality of prototypes in fused deposition modelling. J Mater Process Technol 2001;118(1–3):385–8.
[65] Tyberg J, Bøhn JH. FDM systems and local adaptive slicing. Mater Des 1999;20(2–3):77–82.
[66] Pandey PM, Reddy NV, Dhande SG. Real time adaptive slicing for fused deposition modelling. Int J Mach Tools Manuf 2003;43(1):61–71.
[67] Pandey PM, Reddy NV, Dhande SG. Improvement of surface finish by staircase machining in fused deposition modeling. J Mater Process Technol 2003;132(1–3):323–31.
[68] Thrimurthulu K, Pandey PM, Reddy NV. Optimum part deposition orientation in fused deposition modeling. Int J Mach Tools Manuf 2004;44(6):585–94.
[69] Galantucci L, Lavecchia F, Percoco G. Quantitative analysis of a chemical treatment to reduce roughness of parts fabricated using fused deposition modeling. CIRP Ann 2010;59(1):247–50.
[70] Galantucci LM, Lavecchia F, Percoco G. Experimental study aiming to enhance the surface finish of fused deposition modeled parts. CIRP Ann 2009;58(1):189–92.
[71] Pandey PM, Thrimurthulu K, Reddy NV. Optimal part deposition orientation in FDM by using a multicriteria genetic algorithm. Int J Prod Res 2004;42(19):4069–89.
[72] Gao T, Gillispie GJ, Copus JS, Seol YJ, Atala A, Yoo JJ, et al. Optimization of gelatin–alginate composite bioink printability using rheological parameters: a systematic approach. Biofabrication 2018;10(3):034106.
[73] Chand R, Muhire BS, Vijayavenkataraman S. Computational fluid dynamics assessment of the effect of bioprinting parameters in extrusion bioprinting. Int J Bioprint 2022;8(2):545.
[74] Han S, Kim CM, Jin S, Kim TY. Study of the process-induced cell damage in forced extrusion bioprinting. Biofabrication 2021;13(3):035048.
[75] Ozbolat IT, Hospodiuk M. Current advances and future perspectives in extrusion-based bioprinting. Biomaterials 2016;76:321–43.
[76] Mandrycky C, Wang Z, Kim K, Kim DH. 3D bioprinting for engineering complex tissues. Biotechnol Adv 2016;34(4):422–34.
[77] Bertassoni LE, Cardoso JC, Manoharan V, Cristino AL, Bhise NS, Araujo WA, et al. Direct-write bioprinting of cell-laden methacrylated gelatin hydrogels. Biofabrication 2014;6(2):024105.
[78] Hölzl K, Lin S, Tytgat L, Van Vlierberghe S, Gu L, Ovsianikov A. Bioink properties before, during and after 3D bioprinting. Biofabrication 2016;8(3):032002.
[79] Li H, Liu S, Lin L. Rheological study on 3D printability of alginate hydrogel and effect of graphene oxide. Int J Bioprint 2016;2(2):163–75.
[80] Jia J, Richards DJ, Pollard S, Tan Y, Rodriguez J, Visconti RP, et al. Engineering alginate as bioink for bioprinting. Acta Biomater 2014;10(10):4323–31.
[81] Yin J, Yan M, Wang Y, Fu J, Suo H. 3D bioprinting of low-concentration cell-laden gelatin methacrylate (GelMA) bioinks with a two-step cross-linking strategy. ACS Appl Mater Interfaces 2018;10(8):6849–57.
[82] Liu Q, Yang J, Wang Y, Wu T, Liang Y, Deng K, et al. Direct 3D bioprinting of tough and antifatigue cell-laden constructs enabled by a self-healing hydrogel bioink. Biomacromolecules 2023;24(6):2549–62.
[83] Jongprasitkul H, Turunen S, Parihar VS, Kellomäki M. Sequential cross-linking of gallic acid-functionalized gelma-based bioinks with enhanced printability for extrusion-based 3D bioprinting. Biomacromolecules 2023;24(1):502–14.
[84] Zgeib R, Wang X, Zaeri A, Zhang F, Cao K, Chang RC. Development of a low-cost quad-extrusion 3D bioprinting system for multi-material tissue constructs. Int J Bioprint 2024;10(1):0159.
[85] Hwangbo H, Lee H, Jin EJ, Lee J, Jo Y, Ryu D, et al. Bio-printing of aligned GelMa-based cell-laden structure for muscle tissue regeneration. Bioact Mater 2022;8:57–70.
[86] Ng WL, Yeong WY, Naing MW. Development of polyelectrolyte chitosan-gelatin hydrogels for skin bioprinting. Procedia CIRP 2016;49:105–12.
[87] Skardal A, Zhang J, McCoard L, Oottamasathien S, Prestwich GD. Dynamically crosslinked gold nanoparticle–hyaluronan hydrogels. Adv Mater 2010;22(42):4736–40.
[88] Skardal A, Zhang J, Prestwich GD. Bioprinting vessel-like constructs using hyaluronan hydrogels crosslinked with tetrahedral polyethylene glycol tetracrylates. Biomaterials 2010;31(24):6173–81.
[89] Petta D, Armiento A, Grijpma D, Alini M, Eglin D, D'Este M. 3D bioprinting of a hyaluronan bioink through enzymatic-and visible light-crosslinking. Biofabrication 2018;10(4):044104.
[90] Wang LL, Highley CB, Yeh YC, Galarraga JH, Uman S, Burdick JA. Three-dimensional extrusion bioprinting of single- and double-network hydrogels containing dynamic covalent crosslinks. J Biomed Mater Res A 2018;106(4):86575.
[91] Hockaday L, Kang K, Colangelo N, Cheung P, Duan B, Malone E, et al. Rapid 3D printing of anatomically accurate and mechanically heterogeneous aortic valve hydrogel scaffolds. Biofabrication 2012;4(3):035005.
[92] Fedorovich NE, Swennen I, Girones J, Moroni L, van Blitterswijk CA, Schacht E, et al. Evaluation of photocrosslinked Lutrol hydrogel for tissue printing applications. Biomacromolecules 2009;10(7):1689–96.
[93] Khattak SF, Bhatia SR, Roberts SC. Pluronic F127 as a cell encapsulation material: utilization of membrane-stabilizing agents. Tissue Eng 2005;11(5–6):974–83.
[94] Choudhury D, Tun HW, Wang T, Naing MW. Organ-derived decellularized extracellular matrix: a game changer for bioink manufacturing? Trends Biotechnol 2018;36(8):787–805.
[95] Lowther M, Louth S, Davey A, Hussain A, Ginestra P, Carter L, et al. Clinical, industrial, and research perspectives on powder bed fusion additively manufactured metal implants. Addit Manuf 2019;28:565–84.
[96] Lei P, Qian H, Zhang T, Lei T, Hu Y, Chen C, et al. Porous tantalum structure integrated on Ti6Al4V base by laser powder bed fusion for enhanced bony-ingrowth implants: in vitro and in vivo validation. Bioact Mater 2022;7:3–13.
[97] Chen X, Wu Y, Liu H, Wang Y, Zhao G, Zhang Q, et al. Mechanical performance of PEEK-Ti6Al4V interpenetrating phase composites fabricated by powder bed fusion and vacuum infiltration targeting large and load-bearing implants. Mater Des 2022;215:110531.
[98] Matsko A, Shaker N, Fernandes ACBCJ, Haimeur A, França R. Nanoscale chemical surface analyses of recycled powder for direct metal powder bed fusion Ti-6al-4v root analog dental implant: an X-ray photoelectron spectroscopy study. Bioengineering 2023;10(3):379.
[99] Vanmunster L, D'Haeyer C, Coucke P, Braem A, Van Hooreweder B. Mechanical behavior of Ti6Al4V produced by laser powder bed fusion with engineered open porosity for dental applications. J Mech Behav Biomed Mater 2022;126:104974.
[100] Liu Y, Sing SL, Lim RXE, Yeong WY, Goh BT. Preliminary investigation on the geometric accuracy of 3D printed dental implant using a monkey maxilla incisor model. Int J Bioprint 2022;8(1):476.
[101] Nath SD, Irrinki H, Gupta G, Kearns M, Gulsoy O, Atre S. Microstructure-property relationships of 420 stainless steel fabricated by laser-powder bed fusion. Powder Technol 2019;343:738–46.
[102] Xue L, Atli K, Zhang C, Hite N, Srivastava A, Leff A, et al. Laser powder bed fusion of defect-free NiTi shape memory alloy parts with superior tensile superelasticity. Acta Mater 2022;229:117781.
[103] DebRoy T, Wei HL, Zuback JS, Mukherjee T, Elmer JW, Milewski JO, et al. Additive manufacturing of metallic components–process, structure and properties. Prog Mater Sci 2018;92:112–224.

[104] Yu WH, Sing SL, Chua CK, Kuo CN, Tian XL. Particle-reinforced metal matrix nanocomposites fabricated by selective laser melting: a state of the art review. Prog Mater Sci 2019;104:330–79.
[105] Ishfaq K, Abdullah M, Mahmood MA. A state-of-the-art direct metal laser sintering of Ti6Al4V and AlSi10Mg alloys: surface roughness, tensile strength, fatigue strength and microstructure. Opt Laser Technol 2021;143:107366.
[106] Yuan S, Shen F, Chua CK, Zhou K. Polymeric composites for powder-based additive manufacturing: materials and applications. Prog Polym Sci 2019;91:141–68.
[107] Tan P, Shen F, Tey WS, Zhou K. A numerical study on the packing quality of fibre/polymer composite powder for powder bed fusion additive manufacturing. Virtual Phys Prototyp 2021;16(Suppl1):S1–S.
[108] Chatham CA, Long TE, Williams CB. A review of the process physics and material screening methods for polymer powder bed fusion additive manufacturing. Prog Polym Sci 2019;93:68–95.
[109] Liu B, Li BQ, Li Z. Selective laser remelting of an additive layer manufacturing process on AlSi10Mg. Results Phys 2019;12:982–8.
[110] Demir AG, Previtali B. Investigation of remelting and preheating in SLM of 18Ni300 maraging steel as corrective and preventive measures for porosity reduction. Int J Adv Manuf Technol 2017;93(5–8):2697–709.
[111] Xiong Z, Zhang P, Tan C, Dong D, Ma W, Yu K. Selective laser melting and remelting of pure tungsten. Adv Eng Mater 2020;22(3):1901352.
[112] Chen C, Xiao Z, Zhu H, Zeng X. Distribution and evolution of thermal stress during multi-laser powder bed fusion of Ti-6Al-4 V alloy. J Mater Process Technol 2020;284:116726.
[113] Tsai CY, Cheng CW, Lee AC, Tsai MC. Synchronized multi-spot scanning strategies for the laser powder bed fusion process. Addit Manuf 2019;27:1–7.
[114] Wong H, Dawson K, Ravi G, Howlett L, Jones R, Sutcliffe C. Multi-laser powder bed fusion benchmarking—initial trials with Inconel 625. Int J Adv Manuf Technol 2019;105(7–8):2891–906.
[115] Jaber ST, Hajeer MY, Khattab TZ, Mahaini L. Evaluation of the fused deposition modeling and the digital light processing techniques in terms of dimensional accuracy of printing dental models used for the fabrication of clear aligners. Clin Exp Dent Res 2021;7(4):591–600.
[116] Jindal P, Juneja M, Siena FL, Bajaj D, Breedon P. Mechanical and geometric properties of thermoformed and 3D printed clear dental aligners. Am J Orthod Dentofacial Orthop 2019;156(5):694–701.
[117] Yu X, Li G, Zheng Y, Gao J, Fu Y, Wang Q, et al. 'Invisible'orthodontics by polymeric 'clear'aligners molded on 3D-printed personalized dental models. Regen Biomater 2022;9(1):rbac007.
[118] Vivero-Lopez M, Xu X, Muras A, Otero A, Concheiro A, Gaisford S, et al. Anti-biofilm multi drug-loaded 3D printed hearing aids. Mater Sci Eng C 2021;119:111606.
[119] Lo Russo L, Guida L, Zhurakivska K, Troiano G, Di Gioia C, Ercoli C, et al. Three dimensional printed surgical guides: effect of time on dimensional stability. J Prosthodont 2023;32(5):431–8.
[120] Dalal N, Ammoun R, Abdulmajeed AA, Deeb GR, Bencharit S. Intaglio surface dimension and guide tube deviations of implant surgical guides influenced by printing layer thickness and angulation setting. J Prosthodont 2020;29 (2):161–5.
[121] Ammoun R, Dalal N, Abdulmajeed AA, Deeb GR, Bencharit S. Effects of two postprocessing methods onto surface dimension of in-office fabricated stereolithographic implant surgical guides. J Prosthodont 2021;30(1):71–5.
[122] Rajput M, Mondal P, Yadav P, Chatterjee K. Light-based 3D bioprinting of bone tissue scaffolds with tunable mechanical properties and architecture from photocurable silk fibroin. Int J Biol Macromol 2022;202:644–56.
[123] Tao J, Zhu S, Liao X, Wang Y, Zhou N, Li Z, et al. DLP-based bioprinting of void-forming hydrogels for enhanced stem-cell-mediated bone regeneration. Mater Today Bio 2022;17:100487.
[124] Gao J, Wang H, Li M, Liu Z, Cheng J, Liu X, et al. DLP-printed GelMA-PMAA scaffold for bone regeneration through endocho. Int J Bioprint 2023;9(5):754.
[125] Xie C, Liang R, Ye J, Peng Z, Sun H, Zhu Q, et al. High-efficient engineering of osteo-callus organoids for rapid bone regeneration within one month. Biomaterials 2022;288:121741.
[126] Tao J, Zhu S, Zhou N, Wang Y, Wan H, Zhang L, et al. Nanoparticle-stabilized emulsion bioink for digital light processing based 3D bioprinting of porous tissue constructs. Adv Healthc Mater 2022;11(12):2102810.
[127] Xie X, Wu S, Mou S, Guo N, Wang Z, Sun J. Microtissue-based bioink as a chondrocyte microshelter for dlp bioprinting. Adv Healthc Mater 2022;11 (22):2201877.
[128] Shopperly LK, Spinnen J, Krüger JP, Endres M, Sittinger M, Lam T, et al. Blends of gelatin and hyaluronic acid stratified by stereolithographic bioprinting approximate cartilaginous matrix gradients. J Biomed Mater Res B Appl Biomater 2022;110(10):2310–22.
[129] Breideband L, Wächtershäuser KN, Hafa L, Wieland K, Frangakis AS, Stelzer EH, et al. Upgrading a consumer stereolithographic 3D printer to produce a physiologically relevant model with human liver cancer organoids. Adv Mater Technol 2022;7(10):2200029.
[130] Ma L, Wu Y, Li Y, Aazmi A, Zhou H, Zhang B, et al. Current advances on 3D-bioprinted liver tissue models. Adv Healthc Mater 2020;9(24):2001517.
[131] Grix T, Ruppelt A, Thomas A, Amler AK, Noichl BP, Lauster R, et al. Bioprinting perfusion-enabled liver equivalents for advanced organ-on-a-chip applications. Genes 2018;9(4):176.
[132] Zhou X, Cui H, Nowicki M, Miao S, Lee SJ, Masood F, et al. Three-dimensional-bioprinted dopamine-based matrix for promoting neural regeneration. ACS Appl Mater Interfaces 2018;10(10):8993–9001.
[133] Lee SJ, Nowicki M, Harris B, Zhang LG. Fabrication of a highly aligned neural scaffold via a table top stereolithography 3D printing and electrospinning. Tissue Eng Part A 2017;23(11–12):491–502.
[134] Qiu B, Bessler N, Figler K, Buchholz MB, Rios AC, Malda J, et al. Bioprinting neural systems to model central nervous system diseases. Adv Funct Mater 2020;30(44):1910250.
[135] Cadena M, Ning L, King A, Hwang B, Jin L, Serpooshan V, et al. 3D bioprinting of neural tissues. Adv Healthc Mater 2021;10(15):2001600.
[136] Ng WL, Lee JM, Zhou M, Chen YW, Lee KA, Yeong WY, et al. Vat polymerization-based bioprinting-process, materials, applications and regulatory challenges. Biofabrication 2020;12(2):022001.
[137] Li W, Mille LS, Robledo JA, Uribe T, Huerta V, Zhang YS. Recent advances in formulating and processing biomaterial inks for vat polymerization-based 3D printing. Adv Healthc Mater 2020;9(15):e2000156.
[138] Bartolo P, Gaspar J. Metal filled resin for stereolithography metal part. CIRP Ann 2008;57(1):235–8.
[139] Taormina G, Sciancalepore C, Bondioli F, Messori M. Special resins for stereolithography: in situ generation of silver nanoparticles. Polymers 2018;10(2):212.
[140] Han D, Yang C, Fang NX, Lee H. Rapid multi-material 3D printing with projection micro-stereolithography using dynamic fluidic control. Addit Manuf 2019;27:606–15.
[141] He L, Fei F, Wang W, Song X. Support-free ceramic stereolithography of complex overhanging structures based on an elasto-viscoplastic suspension feedstock. ACS Appl Mater Interfaces 2019;11(20):18849–57.
[142] Halloran JW. Ceramic stereolithography: additive manufacturing for ceramics by photopolymerization. Annu Rev Mater Res 2016;46(1):19–40.
[143] Zhu W, Ma X, Gou M, Mei D, Zhang K, Chen S. 3D printing of functional biomaterials for tissue engineering. Curr Opin Biotechnol 2016;40:103–12.
[144] Bucciarelli A, Paolelli X, De Vitis E, Selicato N, Gervaso F, Gigli G, et al. VAT photopolymerization 3D printing optimization of high aspect ratio structures for additive manufacturing of chips towards biomedical applications. Addit Manuf 2022;60:103200.
[145] Wang Q, Karadas Ö, Backman O, Wang L, Näreoja T, Rosenholm JM, et al. Aqueous two-phase emulsion bioresin for facile one-step 3d microgel-based bioprinting. Adv Healthc Mater 2023;12(19):2203243.
[146] Masuma R, Kashima S, Kurasaki M, Okuno T. Effects of UV wavelength on cell damages caused by UV irradiation in PC12 cells. J Photochem Photobiol B 2013;125:202–8.
[147] Zheng Z, Eglin D, Alini M, Richards GR, Qin L, Lai Y. Visible light-induced 3D bioprinting technologies and corresponding bioink materials for tissue engineering: a review. Engineering 2021;7(7):966–78.
[148] Rouillard AD, Berglund CM, Lee JY, Polacheck WJ, Tsui Y, Bonassar LJ, et al. Methods for photocrosslinking alginate hydrogel scaffolds with high cell viability. Tissue Eng Part C Methods 2011;17(2):173–9.
[149] Huang X, Wang X, Zhao Y. Study on a series of water-soluble photoinitiators for fabrication of 3D hydrogels by two-photon polymerization. Dyes Pigments 2017;141:413–9.
[150] Mironi-Harpaz I, Wang DY, Venkatraman S, Seliktar D. Photopolymerization of cell-encapsulating hydrogels: crosslinking efficiency versus cytotoxicity. Acta Biomater 2012;8(5):183848.
[151] Soman P, Chung PH, Zhang AP, Chen S. Digital microfabrication of user-defined 3D microstructures in cell-laden hydrogels. Biotechnol Bioeng 2013;110(11):3038–47.
[152] Wang Z, Tian Z, Jin X, Holzman JF, Menard F, Kim K. Visible light-based stereolithography bioprinting of cell-adhesive gelatin hydrogels. In: Proceedings of the 39th Annual International Conference of the IEEE Engineering in Medicine and Biology Society (EMBC); 2017 Jul 11–15; Jeju, South Korea. New York City: IEEE; 2017. p. 1599–602.
[153] Gehlen J, Qiu W, Schädli GN, Müller R, Qin XH. Tomographic volumetric bioprinting of heterocellular bone-like tissues in seconds. Acta Biomater 2023;156:49–60.
[154] Lin H, Zhang D, Alexander PG, Yang G, Tan J, Cheng AWM, et al. Application of visible light-based projection stereolithography for live cell-scaffold fabrication with designed architecture. Biomaterials 2013;34(2):331–9.
[155] Rungrojwittayakul O, Kan JY, Shiozaki K, Swamidass RS, Goodacre BJ, Goodacre CJ, et al. Accuracy of 3D printed models created by two technologies of printers with different designs of model base. J Prosthodont 2020;29(2):124–8.
[156] Barbur I, Opris H, Crisan B, Cuc S, Colosi HA, Baciut M, et al. Statistical comparison of the mechanical properties of 3D-printed resin through triple-jetting technology and conventional PMMA in orthodontic occlusal splint manufacturing. Biomedicines 2023;11(8):2155.
[157] Pugalendhi A, Ranganathan R, Chandrasekaran M. Novel fabrication method for clear and hard tooth aligner through additive manufacturing technology: a pilot study. Mater Today Proc 2020;28:551–5.
[158] Goh GD, Sing SL, Lim YF, Thong JLJ, Peh ZK, Mogali SR, et al. Machine learning for 3D printed multi-materials tissue-mimicking anatomical models. Mater Des 2021;211:110125.
[159] Tan L, Wang Z, Jiang H, Han B, Tang J, Kang C, et al. Full color 3D printing of anatomical models. Clin Anat 2022;35(5):598–608.
[160] Mogali SR, Chandrasekaran R, Radzi S, Peh ZK, Tan GJS, Rajalingam P, et al. Investigating the effectiveness of three-dimensionally printed anatomical models compared with plastinated human specimens in learning cardiac and neck anatomy: a randomized crossover study. Anat Sci Educ 2022;15 (6):1007–17.

[161] Kim W, Lee Y, Kang D, Kwak T, Lee HR, Jung S. 3D inkjet-bioprinted lung-on-a-chip. ACS Biomater Sci Eng 2023;9(5):2806–15.
[162] Ng WL, Ayi TC, Liu YC, Sing SL, Yeong WY, Tan BH. Fabrication and characterization of 3d bioprinted triple-layered human alveolar lung models. Int J Bioprint 2021;7(2):332.
[163] Kang D, Park JA, Kim W, Kim S, Lee HR, Kim WJ, et al. All-inkjet-printed 3D alveolar barrier model with physiologically relevant microarchitecture. Adv Sci (Weinh) 2021;8(10):2004990.
[164] Akter F, Araf Y, Promon SK, Zhai J, Zheng C. 3D bioprinting for regenerating covid-19-mediated irreversibly damaged lung tissue. Int J Bioprint 2022;8(4):616.
[165] Shi P, Tan YSE, Yeong WY, Li HY, Laude A. A bilayer photoreceptor-retinal tissue model with gradient cell density design: a study of microvalve-based bioprinting. J Tissue Eng Regen Med 2018;12(5):1297–306.
[166] Sorkio A, Koch L, Koivusalo L, Deiwick A, Miettinen S, Chichkov B, et al. Human stem cell based corneal tissue mimicking structures using laser-assisted 3D bioprinting and functional bioinks. Biomaterials 2018;171:57–71.
[167] Masaeli E, Forster V, Picaud S, Karamali F, Nasr-Esfahani MH, Marquette C. Tissue engineering of retina through high resolution 3-dimensional inkjet bioprinting. Biofabrication 2020;12(2):025006.
[168] Liu H, Wu F, Chen R, Chen Y, Yao K, Liu Z, et al. Electrohydrodynamic jet-printed ultrathin polycaprolactone scaffolds mimicking bruch's membrane for retinal pigment epithelial tissue engineering. Int J Bioprint 2022;8(3):550.
[169] Ng WL, Tan ZQ, Yeong WY, Naing MW. Proof-of-concept: 3D bioprinting of pigmented human skin constructs. Biofabrication 2018;10(2):025005.
[170] Ng WL, Wang S, Yeong WY, Naing MW. Skin Bioprinting: impending reality or fantasy? Trends Biotechnol 2016;34(9):689–99.
[171] Lee V, Singh G, Trasatti JP, Bjornsson C, Xu X, Tran TN, et al. Design and fabrication of human skin by three-dimensional bioprinting. Tissue Eng Part C Methods 2014;20(6):473–84.
[172] Ng WL, Yeong WY. The future of skin toxicology testing – 3D bioprinting meets microfluidics. Int J Bioprint 2019;5(2.1):237.
[173] de Gans BJ, Duineveld PC, Schubert US. Inkjet printing of polymers: state of the art and future developments. Adv Mater 2004;16(3):203–13.
[174] Tekin E, Smith PJ, Schubert US. Inkjet printing as a deposition and patterning tool for polymers and inorganic particles. Soft Matter 2008;4(4):703–13.
[175] Kosmala A, Wright R, Zhang Q, Kirby P. Synthesis of silver nano particles and fabrication of aqueous Ag inks for inkjet printing. Mater Chem Phys 2011;129(3):1075–80.
[176] Raut N, Al-Shamery K. Inkjet printing metals on flexible materials for plastic and paper electronics. J Mater Chem C Mater Opt Electron Devices 2018;6(7):1618–41.
[177] Ni J, Ling H, Zhang S, Wang Z, Peng Z, Benyshek C, et al. Three-dimensional printing of metals for biomedical applications. Mater Today Bio 2019;3:100024.
[178] Derby B. Inkjet printing ceramics: from drops to solid. J Eur Ceram Soc 2011;31(14):2543–50.
[179] Derby B, Reis N. Inkjet printing of highly loaded particulate suspensions. MRS Bull 2003;28(11):815–8.
[180] Cappi B, Özkol E, Ebert J, Telle R. Direct inkjet printing of Si_3N_4: characterization of ink, green bodies and microstructure. J Eur Ceram Soc 2008;28(13):2625–8.
[181] Singh M, Haverinen HM, Dhagat P, Jabbour GE. Inkjet printing-process and its applications. Adv Mater 2010;22(6):673–85.
[182] Park JU, Hardy M, Kang SJ, Barton K, Adair K, Mukhopadhyay DK, et al. High-resolution electrohydrodynamic jet printing. Nat Mater 2007;6(10):782–9.
[183] Fromm JE. Numerical calculation of the fluid dynamics of drop-on-demand jets. IBM J Res Develop 1984;28(3):322–33.
[184] Sun J, Ng JH, Fuh YH, Wong YS, Loh HT, Xu Q. Comparison of micro-dispensing performance between micro-valve and piezoelectric printhead. Microsyst Technol 2009;15(9):1437–48.
[185] Saunders RE, Derby B. Inkjet printing biomaterials for tissue engineering: bioprinting. Int Mater Rev 2014;59(8):430–48.
[186] Li X, Liu B, Pei B, Chen J, Zhou D, Peng J, et al. Inkjet bioprinting of biomaterials. Chem Rev 2020;120(19):10793–833.
[187] Koch L, Gruene M, Unger C, Chichkov B. Laser assisted cell printing. Curr Pharm Biotechnol 2013;14(1):91–7.
[188] Jentsch S, Nasehi R, Kuckelkorn C, Gundert B, Aveic S, Fischer H. Multiscale 3D bioprinting by nozzle-free acoustic droplet ejection. Small Methods 2021;5(6):2000971.
[189] Ng WL, Lee JM, Yeong WY, Win NM. Microvalve-based bioprinting - process, bio-inks and applications. Biomater Sci 2017;5(4):632–47.
[190] Ng WL, Yeong WY, Naing MW. Microvalve bioprinting of cellular droplets with high resolution and consistency. In: Proceedings of the 2nd International Conference on Progress in Additive Manufacturing; 2016 May 17–19; Singapore. Singapore: Nanyang Technological University; 2016. p. 397–402.
[191] Nasehi R, Aveic S, Fischer H. Wall shear stress during impingement at the building platform can exceed nozzle wall shear stress in microvalve-based bioprinting. Int J Bioprint 2023;9(4):743.
[192] Qiu Z, Zhu H, Wang Y, Kasimu A, Li D, He J. Functionalized alginate-based bioinks for microscale electrohydrodynamic bioprinting of living tissue constructs with improved cellular spreading and alignment. Biodes Manuf 2023;6(2):136–49.
[193] Ng WL, Huang X, Shkolnikov V, Goh GL, Suntornnond R, Yeong WY. Controlling droplet impact velocity and droplet volume: key factors to achieving high cell viability in sub-nanoliter droplet-based bioprinting. Int J Bioprint 2021;8(1):424.
[194] Ng WL, Xi H, Shkolnikov V, Suntornnond R, Yeong WY. Polyvinylpyrrolidone-based bioink: influence of bioink properties on printing performance and cell proliferation during inkjet-based bioprinting. Biodes Manuf 2023;6(6):676–90.
[195] Blaeser A, Duarte Campos DF, Puster U, Richtering W, Stevens MM, Fischer H. Controlling shear stress in 3D bioprinting is a key factor to balance printing resolution and stem cell integrity. Adv Healthc Mater 2016;5(3):326–33.
[196] Xu H, Liu J, Zhang Z, Xu C. Cell sedimentation during 3D bioprinting: a mini review. Biodes Manuf 2022;5(3):617–26.
[197] Ng WL, Yeong WY, Naing MW. Polyvinylpyrrolidone-based bio-ink improves cell viability and homogeneity during drop-on-demand printing. Materials 2017;10(2):190.
[198] Huang X, Ng WL, Yeong WY. Predicting the number of printed cells during inkjet-based bioprinting process based on droplet velocity profile using machine learning approaches. J Intell Manuf 2023.
[199] Gudapati H, Dey M, Ozbolat I. A comprehensive review on droplet-based bioprinting: past, present and future. Biomaterials 2016;102:20–42.
[200] Gudapati H, Yan J, Huang Y, Chrisey DB. Alginate gelation-induced cell death during laser-assisted cell printing. Biofabrication 2014;6(3):035022.
[201] Guillotin B, Souquet A, Catros S, Duocastella M, Pippenger B, Bellance S, et al. Laser assisted bioprinting of engineered tissue with high cell density and microscale organization. Biomaterials 2010;31(28):7250–6.
[202] Lee W, Debasitis JC, Lee VK, Lee JH, Fischer K, Edminster K, et al. Multi-layered culture of human skin fibroblasts and keratinocytes through three-dimensional freeform fabrication. Biomaterials 2009;30(8):1587–95.
[203] Lee W, Lee V, Polio S, Keegan P, Lee JH, Fischer K, et al. On-demand three-dimensional freeform fabrication of multi-layered hydrogel scaffold with fluidic channels. Biotechnol Bioeng 2010;105(6):1178–86.
[204] Ng WL, Goh MH, Yeong WY, Naing MW. Applying macromolecular crowding to 3D bioprinting: fabrication of 3D hierarchical porous collagen-based hydrogel constructs. Biomater Sci 2018;6(3):562–74.
[205] Lee JM, Suen SKQ, Ng WL, Ma WC, Yeong WY. Bioprinting of collagen: considerations, potentials, and applications. Macromol Biosci 2021;21(1):2000280.
[206] Umezu S. Precision printing of gelatin utilizing electrostatic inkjet. Jpn. J Appl Phys 2014;53(5S3):05HC01.
[207] Suntornnond R, Ng WL, Huang X, Yeow CHE, Yeong WY. Improving printability of hydrogel-based bio-inks for thermal inkjet bioprinting applications *via* saponification and heat treatment processes. J Mater Chem B Mater Biol Med 2022;10(31):5989–6000.
[208] Koch L, Deiwick A, Franke A, Schwanke K, Haverich A, Zweigerdt R, et al. Laser bioprinting of human induced pluripotent stem cells—the effect of printing and biomaterials on cell survival, pluripotency, and differentiation. Biofabrication 2018;10(3):035005.
[209] Henriksson I, Gatenholm P, Hägg D. Increased lipid accumulation and adipogenic gene expression of adipocytes in 3D bioprinted nanocellulose scaffolds. Biofabrication 2017;9(1):015022.
[210] Lee YC, Zheng J, Kuo J, Acosta-Vélez GF, Linsley CS, Wu BM. Binder jetting of custom silicone powder for direct three-dimensional printing of maxillofacial prostheses. 3D Print Addit Manuf 2022;9(6):520–34.
[211] Meglioli M, Naveau A, Macaluso GM, Catros S. 3D printed bone models in oral and cranio-maxillofacial surgery: a systematic review. 3D Print Med 2020;6(1):30.
[212] Lee G, Carrillo M, McKittrick J, Martin DG, Olevsky EA. Fabrication of ceramic bone scaffolds by solvent jetting 3D printing and sintering: towards load-bearing applications. Addit Manuf 2020;33:101107.
[213] Jo Y, Sarkar N, Bose S. *In vitro* biological evaluation of epigallocatechin gallate (EGCG) release from three-dimensional printed (3DP) calcium phosphate bone scaffolds. J Mater Chem B Mater Biol Med 2023;11(24):5503–13.
[214] Vu AA, Burke DA, Bandyopadhyay A, Bose S. Effects of surface area and topography on 3D printed tricalcium phosphate scaffolds for bone grafting applications. Addit Manuf 2021;39:101870.
[215] Smith M, McGuinness J, O'Reilly M, Nolke L, Murray J, Jones J. The role of 3D printing in preoperative planning for heart transplantation in complex congenital heart disease. Ir J Med Sci 2017;186(3):753–6.
[216] Huotilainen E, Salmi M, Lindahl J. Three-dimensional printed surgical templates for fresh cadaveric osteochondral allograft surgery with dimension verification by multivariate computed tomography analysis. Knee 2019;26(4):923–32.
[217] Ziaee M, Crane NB. Binder jetting: a review of process, materials, and methods. Addit Manuf 2019;28:781–801.
[218] Mostafaei A, Elliott AM, Barnes JE, Li F, Tan W, Cramer CL, et al. Binder jet 3D printing—process parameters, materials, properties, modeling, and challenges. Prog Mater Sci 2021;119:100707.
[219] Santos LC, Condotta R, Ferreira MC. Flow properties of coarse and fine sugar powders. J Food Process Eng 2018;41(2):e12648.
[220] Li L, Zhuo H, Zhu J, Kwan A. Packing density of mortar containing polypropylene, carbon or basalt fibres under dry and wet conditions. Powder Technol 2019;342:433–40.
[221] Seto S, Yagi T, Okuda M, Umehara S, Kataoka M. Lifetime improvement for full-width-array piezo ink jet print head using matrix nozzle arrangement. J Imaging Sci Technol 2009;53(5):50305.

[222] Meisel NA, Williams CB, Druschitz A. Lightweight metal cellular structures via indirect 3D printing and casting. In: Proceedings of the International Solid Freeform Fabrication Symposium; 2012 Aug 6–8; Austin, TX, USA. Austin: University of Texas; 2012. p. 162–76.
[223] Liu J, Rynerson M, inventors. Method for article fabrication using carbohydrate binder. United States patent US 6585930B2. 2003 Jul 1.
[224] Parab ND, Barnes JE, Zhao C, Cunningham RW, Fezzaa K, Rollett AD, et al. Real time observation of binder jetting printing process using high-speed X-ray imaging. Sci Rep 2019;9(1):2499.
[225] Nguyen T, Shen W, Hapgood K. Drop penetration time in heterogeneous powder beds. Chem Eng Sci 2009;64(24):5210–21.
[226] Bai Y, Wagner G, Williams CB. Effect of particle size distribution on powder packing and sintering in binder jetting additive manufacturing of metals. J Manuf Sci Eng 2017;139(8):081019.
[227] Miyanaji H, Yang L. Equilibrium saturation in binder jetting additive manufacturing processes: theoretical model vs. Experimental observations. In: Proceedings of the 26th Annual International Solid Freeform Fabrication Symposium - an Additive Manufacturing Conference; 2015 Aug 10–12; Austin, TX, USA. Austin: University of Texas at Austin; 2016. p. 1945–59.
[228] Banerjee S, Joens C. Debinding and sintering of metal injection molding (MIM) components. In: Handbook of metal injection molding. Amsterdam: Elsevier; 2019. p. 129–71.
[229] Somasundram I, Cendrowicz A, Wilson D, Johns M. Phenomenological study and modelling of wick debinding. Chem Eng Sci 2008;63(14):3802–9.
[230] Mostafaei A, Hughes ET, Hilla C, Stevens EL, Chmielus M. Data on the densification during sintering of binder jet printed samples made from water- and gas-atomized alloy 625 powders. Data Brief 2017;10:116–21.
[231] Güngör F, Ay N. The effect of particle size of body components on the processing parameters of semi transparent porcelain. Ceram Int 2018;44 (9):10611–20.
[232] Liu Z, Sercombe T, Schaffer G. The effect of particle shape on the sintering of aluminum. Metall Mater Trans, A Phys Metall Mater Sci 2007;38(6):1351–7.
[233] Du W, Ren X, Chen Y, Ma C, Radovic M, Pei Z. Model guided mixing of ceramic powders with graded particle sizes in binder jetting additive manufacturing. In: Proceedings of the ASME 2018 13th International Manufacturing Science and Engineering Conference; 2018 Jun 18–22; College Station, TX, USA. Houston: American Society of Mechanical Engineers Digital Collection; 2018.
[234] Kumar A, Bai Y, Eklund A, Williams CB. Effects of hot isostatic pressing on copper parts fabricated via binder jetting. Procedia Manuf 2017;10:935–44.
[235] Lozo B, Stanić M, Jamnicki S, Poljacek SM, Muck T. Three-Dimensional ink jet prints–impact of infiltrants. J Imaging Sci Technol 2008;52(5):51004.
[236] Doyle M, Agarwal K, Sealy W, Schull K. Effect of layer thickness and orientation on mechanical behavior of binder jet stainless steel 420+ bronze parts. Procedia Manuf 2015;1:251–62.
[237] Avila JD, Stenberg K, Bose S, Bandyopadhyay A. Hydroxyapatite reinforced Ti6Al4V composites for load-bearing implants. Acta Biomater 2021;123:379–92.
[238] Ryu DJ, Sonn CH, Hong DH, Kwon KB, Park SJ, Ban HY, et al. Titanium porous coating using 3D direct energy deposition (DED) printing for cementless TKA implants: does it induce chronic inflammation? Materials 2020;13(2):472.
[239] Ryu DJ, Jung A, Ban HY, Kwak TY, Shin EJ, Gweon B, et al. Enhanced osseointegration through direct energy deposition porous coating for cementless orthopedic implant fixation. Sci Rep 2021;11(1):22317.
[240] Afrouzian A, Bandyopadhyay A. 3D printed silicon nitride, alumina, and hydroxyapatite ceramic reinforced Ti6Al4V composites - tailored microstructures to enhance bio-tribo-corrosion and antibacterial properties. J Mech Behav Biomed Mater 2023;144:105973.
[241] Herzog D, Seyda V, Wycisk E, Emmelmann C. Additive manufacturing of metals. Acta Mater 2016;117:371–92.
[242] Jang YH, Ahn DG, Kim J, Kim WS. Re-melting characteristics of a stellite21 deposited part by direct energy deposition process using a pulsed plasma electron beam with a large irradiation area. Int J Precis Eng Manuf-Green Technol 2018;5(4):467–77.
[243] Zhang H, Xu J, Wang G. Fundamental study on plasma deposition manufacturing. Surf Coat Tech 2003;171(1–3):112–8.
[244] Thompson SM, Bian L, Shamsaei N, Yadollahi A. An overview of direct laser deposition for additive manufacturing; part I: transport phenomena, modeling and diagnostics. Addit Manuf 2015;8:36–62.
[245] Hammell JJ, Ludvigson CJ, Langerman MA, Sears JW. Thermal imaging of laser powder deposition for process diagnostics. In: Proceedings of the ASME 2011 International Mechanical Engineering Congress and Exposition; 2011 Nov 11–17; Denver, CO, USA. Houston: American Society of Mechanical Engineers Digital Collection; 2011. p. 41–8.
[246] Raghavan A, Wei H, Palmer T, DebRoy T. Heat transfer and fluid flow in additive manufacturing. J Laser Appl 2013;25(5):052006.
[247] Wang W, Pinkerton A, Wee L, Li L. Component repair using laser direct metal deposition. In: Hinduja S, Fan KC, editors. Proceedings of the 35th International MATADOR Conference; 2007 Jul; Taipei, China. Berlin: Springer; 2007. p. 345–50.
[248] Korinko P, Adams T, Malene S, Gill D, Smugeresky J. Laser engineered net shaping® for repair and hydrogen compatibility. Weld J 2011;90(9):171–81.
[249] Syed WUH, Pinkerton AJ, Li L. Combining wire and coaxial powder feeding in laser direct metal deposition for rapid prototyping. Appl Surf Sci 2006;252 (13):4803–8.
[250] Wang F, Mei J, Wu X. Compositionally graded Ti6Al4V+ TiC made by direct laser fabrication using powder and wire. Mater Des 2007;28(7):2040–6.
[251] Haley JC, Schoenung JM, Lavernia EJ. Modelling particle impact on the melt pool and wettability effects in laser directed energy deposition additive manufacturing. Mater Sci Eng A 2019;761:138052.
[252] Heralić A, Christiansson AK, Lennartson B. Height control of laser metal-wire deposition based on iterative learning control and 3D scanning. Opt Lasers Eng 2012;50(9):1230–41.
[253] Haley JC, Zheng B, Bertoli US, Dupuy AD, Schoenung JM, Lavernia EJ. Working distance passive stability in laser directed energy deposition additive manufacturing. Mater Des 2019;161:86–94.
[254] Wolff SJ, Lin S, Faierson EJ, Liu WK, Wagner GJ, Cao J. A framework to link localized cooling and properties of directed energy deposition (DED)-processed Ti-6Al-4V. Acta Mater 2017;132:106–17.
[255] Lu X, Chiumenti M, Cervera M, Li J, Lin X, Ma L, et al. Substrate design to minimize residual stresses in directed energy deposition AM processes. Mater Des 2021;202:109525.
[256] Mukherjee T, Manvatkar V, De A, DebRoy T. Mitigation of thermal distortion during additive manufacturing. Scr Mater 2017;127:79–83.
[257] Wei H, Mukherjee T, Zhang W, Zuback J, Knapp G, De A, et al. Mechanistic models for additive manufacturing of metallic components. Prog Mater Sci 2021;116:100703.
[258] Szymor P, Kozakiewicz M, Olszewski R. Accuracy of open-source software segmentation and paper-based printed three-dimensional models. J Craniomaxillofac Surg 2016;44(2):202–9.
[259] Gibson I, Rosen D, Stucker B, Khorasani M, Gibson I, Rosen D, et al. Sheet lamination. In: Additive manufacturing technologies. 3rd ed. Berlin: Springer; 2021. p. 253–83.
[260] Gibson I, Rosen D, Stucker B, Khorasani M. Additive manufacturing technologies. Berlin: Springer; 2014.
[261] Murphy SV, Atala A. 3D bioprinting of tissues and organs. Nat Biotechnol 2014;32(8):773–85.
[262] Lewandowski JJ, Seifi M. Metal additive manufacturing: a review of mechanical properties. Annu Rev Mater Res 2016;46(1):151–86.
[263] Pandey P, Reddy NV, Dhande S. Part deposition orientation studies in layered manufacturing. J Mater Process Technol 2007;185(1–3):125–31.
[264] Wang WM, Zanni C, Kobbelt L. Improved surface quality in 3D printing by optimizing the printing direction. In: computer graphics forum. Wiley Online Library; 2016. p. 59–70.
[265] Alharbi N, van de Veen AJ, Wismeijer D, Osman RB. Build angle and its influence on the flexure strength of stereolithography printed hybrid resin material. An in vitro study and a fractographic analysis. Mater Technol 2019;34(1):12–7.
[266] Brika SE, Zhao YF, Brochu M, Mezzetta J. Multi-objective build orientation optimization for powder bed fusion by laser. J Manuf Sci Eng 2017;139 (11):111011.
[267] Das P, Chandran R, Samant R, Anand S. Optimum part build orientation in additive manufacturing for minimizing part errors and support structures. Procedia Manuf 2015;1:343–54.
[268] Frank D, Fadel G. Expert system-based selection of the preferred direction of build for rapid prototyping processes. J Intell Manuf 1995;6(5):339–45.
[269] Lan PT, Chou SY, Chen LL, Gemmill D. Determining fabrication orientations for rapid prototyping with stereolithography apparatus. Comput Aided Des 1997;29(1):53–62.
[270] Zhang Y, De Backer W, Harik R, Bernard A. Build orientation determination for multi-material deposition additive manufacturing with continuous fibers. Procedia CIRP 2016;50:414–9.
[271] Matos MA, Rocha AMA, Pereira AI. Improving additive manufacturing performance by build orientation optimization. Int J Adv Manuf Technol 2020;107(5–6):1–13.
[272] Alexander P, Allen S, Dutta D. Part orientation and build cost determination in layered manufacturing. Comput Aided Des 1998;30(5):343–56.
[273] Masood S, Rattanawong W, Iovenitti P. A generic algorithm for a best part orientation system for complex parts in rapid prototyping. J Mater Process Technol 2003;139(1–3):110–6.
[274] Chacón J, Caminero MA, García-Plaza E, Núnez PJ. Additive manufacturing of PLA structures using fused deposition modelling: effect of process parameters on mechanical properties and their optimal selection. Mater Des 2017;124:143–57.
[275] Simonelli M, Tse YY, Tuck C. Effect of the build orientation on the mechanical properties and fracture modes of SLM Ti–6Al–4V. Mater Sci Eng A 2014;616:1–11.
[276] Das SC, Ranganathan R, Murugan N. Effect of build orientation on the strength and cost of PolyJet 3D printed parts. Rapid Prototyping J 2018;24 (5):832–9.
[277] Reymus M, Fabritius R, Keßler A, Hickel R, Edelhoff D, Stawarczyk B. Fracture load of 3D-printed fixed dental prostheses compared with milled and conventionally fabricated ones: the impact of resin material, build direction, post-curing, and artificial aging-an in vitro study. Clin Oral Investig 2020;24(2):701–10.
[278] Seifi M, Dahar M, Aman R, Harrysson O, Beuth J, Lewandowski JJ. Evaluation of orientation dependence of fracture toughness and fatigue crack propagation behavior of as-deposited ARCAM EBM Ti-6Al-4V. JOM 2015;67 (3):597–607.

[279] Seifi M, Salem A, Beuth J, Harrysson O, Lewandowski JJ. Overview of materials qualification needs for metal additive manufacturing. JOM 2016;68(3):747–64.
[280] Jiang J, Lou J, Hu G. Effect of support on printed properties in fused deposition modelling processes. Virtual Phys Prototyp 2019;14(4):308–15.
[281] Fu YF, Rolfe B, Chiu LN, Wang Y, Huang X, Ghabraie K. Design and experimental validation of self-supporting topologies for additive manufacturing. Virtual Phys Prototyp 2019;14(4):382–94.
[282] Das P, Mhapsekar K, Chowdhury S, Samant R, Anand S. Selection of build orientation for optimal support structures and minimum part errors in additive manufacturing. Comput Aid Des Appl 2017;14(Suppl 1):1–13.
[283] Pham D, Dimov S, Gault R. Part orientation in stereolithography. Int J Adv Manuf Technol 1999;15(9):674–82.
[284] Luo Z, Yang F, Dong G, Tang Y, Zhao YF. Orientation optimization in layer-based additive manufacturing process. In: Proceedings of the ASME 2016 International Design Engineering Technical Conferences and Computers and Information in Engineering Conference; 2016 Aug 21–24, Charlotte, NC, USA. Houston: American Society of Mechanical Engineers Digital Collection; 2016. p. DETC2016-59969, V01AT02A039.
[285] Mirzendehdel AM, Suresh K. Support structure constrained topology optimization for additive manufacturing. Comput Aided Des 2016;81:1–13.
[286] Langelaar M. Combined optimization of part topology, support structure layout and build orientation for additive manufacturing. Struct Multidiscipl Optim 2018;57(5):1985–2004.
[287] Strano G, Hao L, Everson R, Evans K. A new approach to the design and optimisation of support structures in additive manufacturing. Int J Adv Manuf Technol 2013;66(9–12):1247–54.
[288] Hussein A, Hao L, Yan C, Everson R, Young P. Advanced lattice support structures for metal additive manufacturing. J Mater Process Technol 2013;213(7):1019–26.
[289] Cheng L, To A. Part-scale build orientation optimization for minimizing residual stress and support volume for metal additive manufacturing: theory and experimental validation. Comput Aided Des 2019;113:1–23.
[290] Mirzababaei S, Paul BK, Pasebani S. Metal powder recyclability in binder jet additive manufacturing. JOM 2020;72(9):3070–9.
[291] Strondl A, Lyckfeldt O, Brodin H, Ackelid U. Characterization and control of powder properties for additive manufacturing. JOM 2015;67(3):549–54.
[292] Su CY, Wang JC, Chen DS, Chuang CC, Lin CK. Additive manufacturing of dental prosthesis using pristine and recycled zirconia solvent-based slurry stereolithography. Ceram Int 2020;46(18):287019.
[293] Ratner BD, Latour RA. Role of water in biomaterials. In: Biomaterials science: an Introduction to materials in medicine. Amsterdam: Elsevier; 2020. p. 77–82.
[294] Berg JM, Tymoczko JL, Stryer L. Biochemistry. New York City: Freeman and Company; 2002.
[295] Goh CS, Lan N, Douglas SM, Wu B, Echols N, Smith A, et al. Mining the structural genomics pipeline: identification of protein properties that affect high-throughput experimental analysis. J Mol Biol 2004;336(1):115–30.
[296] Asherie N. Protein crystallization and phase diagrams. Methods 2004;34(3):266–72.
[297] Moran LA, Horton RA, Scrimgeour KG, Perry MD. Principles of biochemistry. 6th ed. Cambridge: Pearson; 2014.
[298] Narayan R. Biomedical materials. 2nd ed. Berlin: Springer; 2021.
[299] Harding JL, Reynolds MM. Combating medical device fouling. Trends Biotechnol 2014;32(3):140–6.
[300] Firkowska-Boden I, Zhang X, Jandt KD. Controlling protein adsorption through nanostructured polymeric surfaces. Adv Healthc Mater 2018;7(1):1700995.
[301] Michael KE, Vernekar VN, Keselowsky BG, Meredith JC, Latour RA, García AJ. Adsorption-induced conformational changes in fibronectin due to interactions with well-defined surface chemistries. Langmuir 2003;19(19):8033–40.
[302] Kowalczyńska HM, Nowak-Wyrzykowska M, Dobkowski J, Kołos R, Kamiński J, Makowska-Cynka A, et al. Adsorption characteristics of human plasma fibronectin in relationship to cell adhesion. J Biomed Mater Res 2002;61(2):260–9.
[303] Shen M, Horbett TA. The effects of surface chemistry and adsorbed proteins on monocyte/macrophage adhesion to chemically modified polystyrene surfaces. J Biomed Mater Res 2001;57(3):336–45.
[304] Li T, Hao L, Li J, Du C, Wang Y. Insight into vitronectin structural evolution on material surface chemistries: the mediation for cell adhesion. Bioact Mater 2020;5(4):1044–52.
[305] Alberts B, Johnson A, Lewis J, Raff M, Roberts K, Walter P. General principles of cell communication. In: molecular biology of the cell. 4th ed. Oxford: Garland Science; 2002.
[306] Geiger B, Bershadsky A, Pankov R, Yamada KM. Transmembrane crosstalk between the extracellular matrix-cytoskeleton crosstalk. Nat Rev Mol Cell Biol 2001;2(11):793–805.
[307] Wei Q, Haag R. Universal polymer coatings and their representative biomedical applications. Mater Horiz 2015;2(6):567–77.
[308] Sperling C, Schweiss RB, Streller U, Werner C. In vitro hemocompatibility of self-assembled monolayers displaying various functional groups. Biomaterials 2005;26(33):6547–57.
[309] Absolom DR, Zingg W, Neumann AW. Protein adsorption to polymer particles: role of surface properties. J Biomed Mater Res 1987;21(2):161–71.
[310] Lord MS, Foss M, Besenbacher F. Influence of nanoscale surface topography on protein adsorption and cellular response. Nano Today 2010;5(1):66–78.
[311] Harvey AG, Hill EW, Bayat A. Designing implant surface topography for improved biocompatibility. Expert Rev Med Devices 2013;10(2):257–67.
[312] Scopelliti PE, Borgonovo A, Indrieri M, Giorgetti L, Bongiorno G, Carbone R, et al. The effect of surface nanometre-scale morphology on protein adsorption. PLoS One 2010;5(7):e11862.
[313] Gu Z, Yang Z, Chong Y, Ge C, Weber JK, Bell DR, et al. Surface curvature relation to protein adsorption for carbon-based nanomaterials. Sci Rep 2015;5(1):10886.
[314] Roach P, Farrar D, Perry CC. Surface tailoring for controlled protein adsorption: effect of topography at the nanometer scale and chemistry. J Am Chem Soc 2006;128(12):3939–45.
[315] Williams DF. Definitions in biomaterials: progress in biomedical engineering. Biomaterials 1987;10:216–38.
[316] Bernard M, Jubeli E, Pungente MD, Yagoubi N. Biocompatibility of polymer-based biomaterials and medical devices - regulations, in vitro screening and risk-management. Biomater Sci 2018;6(8):2025–53.
[317] Thevenot P, Hu W, Tang L. Surface chemistry influences implant biocompatibility. Curr Top Med Chem 2008;8(4):270–80.
[318] ISO 10993–5: biological evaluation of medical devices - part 5: tests for in vitro cytotoxicity. ISO standard. Geneva: International Standard Organization; 2009.
[319] Pizzoferrato A, Ciapetti G, Stea S, Cenni E, Arciola CR, Granchi D, et al. Cell culture methods for testing biocompatibility. Clin Mater 1994;15(3):173–90.
[320] Kirkpatrick CJ, Bittinger F, Wagner M, Köhler H, van Kooten TG, Klein CL, et al. Current trends in biocompatibility testing. Proc Inst Mech Eng H 1998;212(2):75–84.
[321] van Meerloo J, Kaspers GJ, Cloos J. Cell sensitivity assays: the MTT assay. In: Cree IA, editor. Cancer cell culture methods and protocols. Berlin: Springer; 2011. p. 237–45.
[322] Herath I, Davies J, Will G, Tran PA, Velic A, Sarvghad M, et al. Anodization of medical grade stainless steel for improved corrosion resistance and nanostructure formation targeting biomedical applications. Electrochim Acta 2022;416:140274.
[323] Yildiz F, Yetim A, Alsaran A, Efeoglu I. Wear and corrosion behaviour of various surface treated medical grade titanium alloy in bio-simulated environment. Wear 2009;267(5–8):695–701.
[324] Chang HY, Tuan WH, Lai PL. Biphasic ceramic bone graft with biphasic degradation rates. Mater Sci Eng C 2021;118:111421.
[325] Armentano I, Dottori M, Fortunati E, Mattioli S, Kenny J. Biodegradable polymer matrix nanocomposites for tissue engineering: a review. Polym Degrad Stabil 2010;95(11):2126–46.
[326] Lyu S, Untereker D. Degradability of polymers for implantable biomedical devices. Int J Mol Sci 2009;10(9):4033–65.
[327] Pakshir P, Younesi F, Wootton KA, Battiston K, Whitton G, Ilagan B, et al. Controlled release of low-molecular weight, polymer-free corticosteroid coatings suppresses fibrotic encapsulation of implanted medical devices. Biomaterials 2022;286:121586.
[328] Welch NG, Winkler DA, Thissen H. Antifibrotic strategies for medical devices. Adv Drug Deliv Rev 2020;167:109–20.
[329] Barchowsky A. Systemic and immune toxicity of implanted materials. In: Biomaterials science: an introduction to materials in medicine. 4th ed. Amsterdam: Elsevier; 2020. p. 791–9.
[330] Zopf DA, Hollister SJ, Nelson ME, Ohye RG, Green GE. Bioresorbable airway splint created with a three-dimensional printer. N Engl J Med 2013;368(21):2043–5.
[331] Morrison RJ, Hollister SJ, Niedner MF, Mahani MG, Park AH, Mehta DK, et al. Mitigation of tracheobronchomalacia with 3D-printed personalized medical devices in pediatric patients. Sci Transl Med 2015;7(285):285ra64.
[332] Dzian A, Živčák J, Penciak R, Hudák R. Implantation of a 3D-printed titanium sternum in a patient with a sternal tumor. World J Surg Oncol 2018;16(1):7.
[333] Cruz RLJ, Ross MT, Powell SK, Woodruff MA. Advancements in soft-tissue prosthetics part A: the art of imitating life. Front Bioeng Biotechnol 2020;8:121.
[334] Nutt D, Chronicle C. Cornellian-founded company implants 3D-bioprinted ear [Internet]. College Avelthaca: Cornell Chronicle; 2022 Jun 2 [Cited 2024 Feb 7]. Available from: https://news.cornell.edu/stories/2022/06/cornellian-founded-company-implants-3d-bioprinted-ear.
[335] Fogarasi M, Snodderly KL, Di Prima MA. A survey of additive manufacturing trends for FDA-cleared medical devices. Nat Rev Bioeng 2023;1:687–9.
[336] Valls-Esteve A, Lustig-Gainza P, Adell-Gomez N, Tejo-Otero A, Englí-Rueda M, Julian-Alvarez E, et al. A state-of-the-art guide about the effects of sterilization processes on 3D-printed materials for surgical planning and medical applications: a comparative study. Int J Bioprint 2023;9(5):756.
[337] Told R, Ujfalusi Z, Pentek A, Kerenyi M, Banfai K, Vizi A, et al. A state-of-the-art guide to the sterilization of thermoplastic polymers and resin materials used in the additive manufacturing of medical devices. Mater Des 2022;223:111119.
[338] Rogers W. Steam and dry heat sterilization of biomaterials and medical devices. In: Lerouge S, Simmons A, editors. Sterilisation of biomaterials and medical devices. Amsterdam: Elsevier; 2012. p. 20–55.
[339] Harrell CR, Djonov V, Fellabaum C, Volarevic V. Risks of using sterilization by gamma radiation: the other side of the coin. Int J Med Sci 2018;15(3):274–9.
[340] McEvoy B, Rowan NJ. Terminal sterilization of medical devices using vaporized hydrogen peroxide: a review of current methods and emerging opportunities. J Appl Microbiol 2019;127(5):1403–20.
[341] Shintani H. Ethylene oxide gas sterilization of medical devices. Biocontrol Sci 2017;22(1):1–16.

[342] Mousavi SM, Shamohammadi M, Moradi M, Hormozi E, Rakhshan V. Effects of cold chemical (glutaraldehyde) versus autoclaving sterilization on the rate of coating loss of aesthetic archwires: a double-blind randomized clinical trial. Int Orthod 2020;18(2):380–8.

[343] Dizon JRC, Espera Jr AH, Chen Q, Advincula RC. Mechanical characterization of 3D-printed polymers. Addit Manuf 2018;20:44–67.

[344] Gibson I, Rosen D, Stucker B, Khorasani M, Rosen D, Stucker B, et al. Chapter 16: post-processing. In: Additive manufacturing technologies. Berlin: Springer; 2021. p. 457–89.

[345] Tamburrino F, Barone S, Paoli A, Razionale A. Post-processing treatments to enhance additively manufactured polymeric parts: a review. Virtual Phys Prototyp 2021;16(2):221–54.